UC Berkeley
UC Berkeley Electronic Theses and Dissertations

Title

Dynamic Trafficking of Melanocortin 4 Receptor at the Primary Cilium Reflects Energy Homeostasis

Permalink

https://escholarship.org/uc/item/1z73w6p3

Author

Yue, Xinyu

Publication Date

2024

Peer reviewed|Thesis/dissertation

eScholarship.org Powered by the California Digital Library
University of California

“Dynamic Trafficking of Melanocortin 4 Receptor at the Primary Cilium Reflects Energy Homeostasis”

By

Annie Yue

A dissertation submitted in partial satisfaction of the

requirements for the degree of

Doctor of Philosophy

in

Metabolic Biology

in the

Graduate Division

of the

University of California, Berkeley

Committee in Charge:

Professor Jen-Chywan Wang, Chair

Professor Christian Vaisse

Professor Andreas Stahl

Summer 2024

Abstract

"Dynamic Trafficking of Melanocortin 4 Receptor at the Primary Cilium Reflects Energy Homeostasis"

By

Annie Yue

Doctor of Philosophy in Metabolic Biology

University of California, Berkeley

Jen-Chywan Wang, Chair

Mutations in the melanocortin 4 receptor (MC4R) are the leading cause of monogenic obesity. MC4R is a key player in the leptin melanocortin pathway, which regulates long term energy homeostasis. Mutations in anorexigenic components of this pathway leads to monogenic obesity. However, the method in which this pathway encodes, and stores body weight set point, thus energy homeostasis, is unknown.

In chapter 1, we will characterize and validate two different knock-in mouse models that will allow for studying MC4R localization and specific manipulation of MC4R neurons.

In chapter 2, we will show how dynamic localization of MC4R encodes information on peripheral energy stores by integrating information from upstream components of the leptin melanocortin pathway.

Table of Contents

Abstract **1**
Table of Contents ..... **i**
List of Figures ..... **iv**
Dedication ..... **v**
Acknowledgements ..... **vi**
Chapter 0: General Introduction ..... **vii**
Genetics and Obesity vii
Leptin melanocortin pathway and the regulation of long-term energy homeostasis vii
Leptin and leptin receptor viii
First order neurons: AGRP and POMC neurons in the arcuate nucleus viii
Second order neurons: MC4R neurons in the paraventricular nucleus ix
Primary cilia are involved in the regulation of long-term energy homeostasis xi
Ciliopathies with obesity as a clinical feature xi
Other ciliary genes associated with obesity xii
Neuronal Communication: Synaptic vs Volumetric xiii
Figures xiv
Transition xvii
Chapter 1: Characterization of mouse models **2**
Summary 2
Introduction 3
Results 3
Generation and Validation of *Mc4r-t2a-Cre* mice 3
Generation and Validation of *Mc4r-eGfp* mice 3
Assessing MC4R and MRAP2 colocalization throughout the brain 4
Discussion 4
Figures 6
Methods 12
Animals 12

Generation of knock-in mice 12
Direct fluorescence and immunofluorescence studies of the mouse brain 12
RNAScope 13
Image capturing and processing 13
Transition 14
Chapter 2: Molecular encoding of peripheral energy levels by neuronal cilia 15
Summary 15
Introduction 16
Results 17
Fasting leads to accumulation of MC4R at primary cilia 17
MC4R localization to primary cilia of PVN^{MC4R} neurons correlates with energy deficit 17
MC4R accumulation at PVN^{MC4R} neuronal cilia is leptin dependent 18
AGRP is required for peripheral energy stores and leptin control of MC4R localization to cilia 18
AGRP drives MC4R accumulation at primary cilia of PVN^{MC4R} neurons in adult mice 19
AGRP mediated increase in MC4R localization to primary cilia is cell autonomous 19
Anatomical differences in MC4R enrichment at cilia at increasing levels of energy-deficit 20
Discussion 20
Figures 22
Methods 43
Animals 43
Mouse metabolism studies 43
Pharmacological agents 43
Pump implantations 43
Subcutaneous leptin pump implantations 43
Intracerebroventricular AGRP infusion 44
Diphtheria toxin injections 44
Serum leptin measurements 44
Brain imaging 44
Image analysis of brain sections 45

Training of convolutional neural network-based segmentation models for primary cilia segmentation into maximum projection of 60x brain images 46
Automated quantification of MC4R localization at the primary cilium in brain 46
Validation of the NIS.ai cilia segmentation algorithm 47
Assessment of ligand dependent MC4R localization in cell culture 48
Quantification of statistical analysis 49
Chapter 3: Final conclusions and future directions **55**
References **53**

List of Figures

0.1 The leptin melanocortin pathway ..... **xiv**

0.2 Primary cilia structure and components ..... **xv**

0.3 Synaptic vs volumetric signaling ..... **xvi**

1.1 Characterization and validation of *Mc4r-t2a-Cre* allele **6**

1.2 *Mc4r-eGfp* allele design and verification **8**

1.3 MC4R colocalization with MRAP2 at neuronal primary cilium in select nuclei **10**

2.1 Fasting increases MC4R localization to the primary cilium **22**

2.2 MC4R enrichment at primary cilia mirrors energy deficit **24**

2.3 Leptin increases ciliary MC4R level **26**

2.4 AGRP is required for MC4R accumulation at primary cilia **28**

2.5 AGRP is required to promote MC4R accumulation in primary cilia of leptin-deficient mice . **29**

2.6 AGRP drives MC4R accumulation at primary cilia in vivo and cell-autonomously **31**

2.7 Anatomical differences in MC4R ciliary enrichment with increasing levels of energy-deficit **33**

2.8 Supplemental Figure S1: Quantification of ciliary MC4R localization using AI segmentation models. **35**

2.9 Supplemental Figure S2: Validation of automated cilia segmentation process. **37**

2.10 Supplemental Figure S3: Body weight change upon energy deficit. **39**

2.11 Supplemental Figure S4: Circulating leptin levels upon energy deficit. **40**

2.12 Supplemememental Figure S5: Body weight change of $Lep^{ob/ob}$ $Mc4r^{Gfp/Gfp}$ mice infused with vehicle or leptin. **40**

2.13 Supplemental Figure S6: Body weight change of mice with conditional loss of AGRP neurons. **41**

2.14 Supplemental Figure S7: Body weight change of aCSF- and AGRP- infused mice. **41**

2.15 Supplemental Figure S8: AGRP does not change cilia length. **42**

3.1 Neuronal encoding of energy homeostasis. **52**

Dedication

There are so many people who contributed to my success and motivated me to do my best through my PhD journey. I'd like to dedicate my thesis to you all.

To members of my cohort who joined the Metabolic Biology Program in the same year that I did, and the friends I've made in the Nutritional Science and Toxicology Department. You all kept me connected to Berkeley and helped me navigate PhD life.

To my mentors, Adelaide Bernard, and Francois Mifsud; and my PI, Christian Vaisse, for teaching me and providing me with everything I needed to succeed and for inspiring me inside and outside of lab.

To all of my lab members, past and present, for creating such a welcoming and supportive environment.

And, of course, to my family for supporting me throughout my educational career.

Acknowledgements

Chapter 1 adapted with permission from Journal of Clinical Investigation and Journal of Clinical Investigation Insights

J Clin Invest 2021 May 3;131(9):e142064; https://doi.org/10.1172/JCI142064..

Melanocortin-4 receptor signals at the neuronal primary cilium to control food intake and body weight.

Yi Wang*, Adelaide Bernard*, Fanny Comblain*, Xinyu Yue, Christophe Paillart, Sumei Zhang, Jeremy F. Reiter, Christian Vaisse

JCI Insight. 2023;8(2):e155900. https://doi.org/10.1172/jci.insight.155900.

MRAP2 regulates energy homeostasis by promoting primary cilia localization of MC4R.

Adelaide Bernard, Irene Ojeda Naharros, Zinyu Yue, Francois Mifsud, Abbey Blake, Florence Guglielmetti, Jordi Ciprin, Sumei Zhang, Erin McDaid, Kellan Kim, Maxence V Nachury, Jeremy Reiter, and Christian Vaisse

Chapter 0: General Introduction

Genetics and obesity

The prevalence of obesity has increased worldwide throughout the years. Approximately 42% of the American population currently has obesity which is a risk factor for type 2 diabetes, hypertension, sleep disorders, and cardiovascular disease[1]. Although Ozempic/Wegovy has surged to popularity as a "magic bullet" against obesity, the resulting weight loss does not last after the drug is no longer used.[1,2] Thus, understanding the way that our bodies encode long term information on peripheral energy stores and adjust energy intake and expenditure in response is essential in tackling the obesity epidemic.

Obesity is the result of the interaction between environment and genetics.[3] Twin studies, and adoption studies demonstrate that 40-70% of human variation in body mass index can be accounted for by genetic factors.[4,5] Both rare and common genetic variants contribute to human susceptibility to obesity. Interestingly, genome wide association studies the second strongest obesity associated SNP is located at melanocortin 4 receptor (MC4R) locus[6–9]. MC4R is a key player in the leptin melanocortin pathway. Mutations in genes involved in this pathway (including MC4R) leads to monogenic obesity, which underscores the importance of this pathway in body weight regulation and demonstrates that obesity is much more than the result of poor lifestyle choices[10].

Leptin melanocortin pathway and the regulation of long-term energy homeostasis

Set point theory is a model for long term energy regulation. It states that there is an active feedback mechanism that maintains a set level of energy stores ("set point"). When energy stores are higher than the set point, energy expenditure is increased, and food intake is decreased which leads to a decrease in energy stores until it reaches the set point. More importantly, this system is in place to ensure adequate calorie intake. When energy stores are lower than the set point, energy expenditure is decreased and food intake is increased to replenish energy stores back to the set point[11,12]. The discovery of leptin provides strong molecular underpinning for the set point theory.

The leptin melanocortin pathway is a highly conserved pathway designed to adapt energy expenditure and food intake to the organism's energy stores (Figure 1). Leptin is produced and secreted into the blood by white adipocytes in proportion to fat mass[13]. Leptin travels through the circulatory system where it eventually binds to its receptor in the arcuate nucleus of the hypothalamus (ARC). Leptin then binds to its receptors on two different neuronal subpopulations: agouti related peptide (AGRP) neurons and proopiomelanocortin (POMC) neurons. Leptin affects these subpopulations in opposite ways: POMC neurons are activated whereas AGRP neurons are

inhibited. These first order neurons project to second order neurons in the paraventricular nucleus: MC4R neurons. Activation of POMC neurons results in an increased production of POMC which will be cleaved by proconvertase 1 and 2 to produce alpha melanocyte stimulating hormone (α-MSH), which activates MC4R. Activation of MC4R leads to inhibition of food intake[14]. In settings of long term caloric deficit, fat stores decrease, which leads to a decrease in leptin secretion from white adipocytes[15]. When low levels of leptin are in blood circulation, AGRP neurons are activated which results in the inhibition of MC4R neurons thus promoting food intake. The following subsections will go into aspects of the leptin melanocortin pathway in greater detail[14].

Leptin and leptin receptor

The leptin deficient (*ob/ob*) and leptin receptor knock out (*db/db*) mouse models were discovered in 1950 and 1965 respectively[16]. The ob/ob mouse is obese, hyperphagic, infertile, has decreased corticosteroid levels, hypothermic, diabetic, and have altered immune and hematologic function[15,16]. The db/db mouse is phenotypically similar to the ob/ob mouse, it is characterized by obesity, hyperphagia, and severe diabetes[16]. Parabiosis experiments showed that the ob/ob mouse was lacking in a satiety factor and the db/db mouse was lacking in the receptor for a satiety factor[15,16]. The satiety factor was identified and cloned from the ob mouse; and the leptin receptor was identified shortly after[17,18].

Leptin is a hormone that is produced by adipose tissue in proportion to the amount of fat stored: more fat stored means increased levels of circulating leptin[13]. Not only do leptin levels fluctuate with weight, it also fluctuates on a circadian rhythm to a lesser extent[19]. Mutations in leptin causes monogenic obesity in humans which can be treated by leptin replacement therapy[16]. Leptin affects multiple neural circuits, including those involved in the control of mood, reproduction, activity, thermoregulation, stress and food intake[15].

There are 6 isoforms of the leptin receptor (LEPRa-f) as a result of alternative splicing of the *Lepr* gene. Leprb is the long form of the leptin receptor and is responsible for the effects of leptin on energy homeostasis. Leptin receptors are found in the regions in the brainstem (nucleus tractus solitarii and area postrema), and the hypothalamus (arcuate nucleus, lateral hypothalamus, ventromedial hypothalamus, dorsal medial hypothalamus)[20]. Leptin binding to LEPRb activates the JAK2/STAT3 pathway[19]. Once activated, leptin receptors traffic to the periciliary area around primary cilia. Impaired LEPR localization to the periciliary area blunts STAT3 leptin signaling[21].

First order neurons: AGRP and POMC neurons in the arcuate nucleus

AGRP neurons located in the arcuate nucleus of the brain exerts orexigenic effects on the body[22]. Deletion of AGRP neurons in adult mice results in decreased body weight due to the lack of food intake until the point of starvation[23–25]. Thus, AGRP neurons are necessary for food intake. Overexpression of *Agrp* leads to hyperphagia, however germinal deletion of *Agrp* does not result in a noticeable phenotype[26]. This is because there are compensatory mechanisms that also signal

hunger[27]. Optogenetic and chemogenetic activation of AGRP neurons results in feeding, even in satiated mice[27–29]. AGRP neurons are necessary and sufficient for feeding.

AGRP neurons sense multiple circulatory hormones that signal peripheral energy status including leptin and insulin, which inhibit these neurons; and ghrelin, which activates these neurons. When AGRP neurons are activated, they signal hunger by secreting multiple neuromediators: gamma aminobutyric acid (GABA), which binds to $GABA_A$ and $GABA_B$ receptors; AGRP, which binds to MC3R and MC4R; and neuropeptide Y (NPY), which a family of receptors, NPY1-5R. GABA mediates acute feeding. NPY mediates intermediate (1 hour) feeding. AGRP is responsible for inducing long term increases in feeding[22]. In addition to feeding, AGRP neurons have a role in energy expenditure. A recent paper demonstrated an ARC^{AGRP} neuron connection to MC4R neurons in the dorsal lateral dorsal raphe nucleus (dlDRN) to inguinal brown adipose tissue and subcutaneous adipose tissue circuit that mediates thermogenesis after a meal[30].

AGRP neurons project to multiple brain regions: bed nucleus of the stria terminalis (BNST), paraventricular nucleus of the hypothalamus (PVN), paraventricular thalamic nucleus (PVT), lateral hypothalamus (LH), parabrachial nucleus (PB), and even to other neurons in the ARC[31]. AGRP neurons can inhibit neuron activation in these locations via synaptic GABA secretion. AGRP is located in extra synaptic vesicles along axonal projections and are secreted extrasynaptically[32].

POMC neurons are heterogeneous in function and expression[33]. Expression of the proopiomelanocortin (POMC) gene leads to the production of a pro-hormone which is cleaved into multiple peptides that are released including: adrenocorticotropic hormone (ACTH); α-, β-, γ- melanocyte stimulating hormones (αMSH, βMSH, γMSH); corticotropin like intermediate peptide (CLIP) and β endorphin. These peptides are released to function in pathways involving: pigmentation, adrenocortical function, reward, sexual behaviour, immunity and regulation of energy metabolism. However, ARC^{POMC} neurons only secrete αMSH. Specifically, αMSH binds and activates MC4R in order to inhibit food intake[34]. Null mutations in Pomc lead to hyperphagia, obesity, adrenal deficiency and red hair in humans[35]. *Pomc*$^{-/-}$ mice exhibit hyperphagia, obesity, adrenal development defects, and altered pigmentation[36]. Deletion of *Leprb* in POMC neurons leads to hyperleptinemia and obesity, however, re-expression of *Pomc* only in LEPRb neurons is sufficient to rescue obesity in *Pomc* null mice[37,38]. Interestingly, chronic activation of POMC neurons, and over expression of *Pomc* in wild type mice fails to prevent or reverse obesity[39].

Second order neurons: MC4R neurons in the paraventricular nucleus

Human mutations in *MC4R* lead to severe early-onset obesity due to hyperphagia and reduced energy expenditure[40]. Mutations in *MC4R* are the cause of 2.5-5% of all early-onset obesity and/or adult class 3 obesity[41–44]. *Mc4r*$^{-/-}$ mice are obese, hyperphagic, have lower energy expenditure, and perturbed glucose homeostasis thus they recapitulate the phenotype of humans with *MC4R* null mutations. *Mc4r*$^{+/-}$ mice are haploinsufficient, thus have a body weight

phenotype that is between wildtype mice and *Mc4r*$^{-/-}$ mice. Thus, a functional MC4R is important for controlling energy balance.

Rescue of *Mc4r* only in the PVN of *Mc4r* null mice results in partial rescue of the obesity phenotype, thus demonstrating that *Mc4r* in the PVN is sufficient to control food intake, and MC4R neurons in other regions of the brain is responsible for controlling energy expenditure[45,46]. Deletion of Mc4r in just the PVN results in hyperphagia and obesity[47]. Thus, although MC4R neurons are located in multiple regions in the brain, PVN^{MC4R} neurons are necessary and sufficient for controlling food intake and energy homeostasis.

Consistent with observations in genetic mouse models, chemogenetic activation of MC4R neurons results in decreased food intake, whereas chemogenetic inhibition of MC4R neurons results in increased food intake[48]. Infusion of MC4R agonist results in decreased food intake, increased energy expenditure and weight loss[49–51]. Central administration of MC4R antagonists increase food intake, energy conservation, and weight gain[52,53]. Interestingly, chronic activation of MC4R neurons, or overexpression of MC4R fails to prevent or reverse obesity, suggesting that melanocortin action is biased against weight loss[39].

PVN^{MC4R} neurons project to the lateral parabrachial nucleus (LPBN) and the dorsal motor vagus (DMV)[48]. LPBN neurons downstream of PVN^{MC4R} neurons are glutamatergic. Neurons in the LPBN receive innervations from ascending sensory afferents (vagal and spinal) thus it is possible that this population integrates ingestion related visceral stimuli and hypothalamic homeostatic information to adapt food intake.

MC4R is a seven transmembrane $G_{\alpha s}$-protein coupled receptor. It is part of a family of 5 receptors (MC1-5R). Unlike many GPCRs, MC4R has both an agonist, αMSH, and antagonist, AGRP. When activated, MC4R will activate adenylyl cyclase which increases intracellular cAMP levels[14]. Null mutation in adenylyl cyclase 3 (ADCY3), which colocalizes with MC4R in mice, result in severe monogenic obesity[54,55]. Recently, it has been demonstrated that MC4R localizes to the primary cilia of neurons in the PVN[54,56]. Deletion of primary cilia from MC4R neurons results in hyperphagia and obesity and the inability of these mice to respond to melanotan II (MTII), an agonist for MC4R. Suppression of G_s signaling in the primary cilia of PVN^{MC4R} neurons also results in hyperphagia and obesity. Thus, primary cilia in PVN^{MC4R} neurons, and G_s signaling in these primary cilia are necessary for PVNMC4R neurons to signal satiety and control energy homeostasis[56,57].

Melanocortin receptors interact with a family of single-pass transmembrane proteins accessory proteins called melanocortin receptor associated proteins (MRAP1 and MRAP2). MRAP2 interacts with MC4R and was shown to increase ligand sensitivity and MC4R mediated generation of cAMP in non-ciliated heterologous systems[58]. *MRAP2* variants were found in patients with obesity[59–62]. *Mrap2*$^{-/-}$ mice develop severe obesity[62]. We have demonstrated that MRAP2 is

necessary for MC4R localization to the primary cilium. When MC4R cannot localize to the primary cilium due to deletion of *Mrap2* in MC4R neurons, mice are hyperphagic and obese[63].

Primary cilia are involved in the regulation of long-term energy homeostasis

Primary cilia are sensory organelles that protrude from the cell surface. Most mammalian cells have a primary cilium. Primary cilia were once thought of as vestigial organelles, but are now known to be involved in sensing external cues and conveying signals to regulate a variety of physiological pathways. Primary cilia are highly conserved and are involved in embryonic development, and tissue homeostasis. Dysfunction in the structure or function of primary cilia results in a family of diseases collectively known as ciliopathies[64]. Ciliopathies are pleiotropic and can result in a variety of symptoms such as: infertility, polydactylyl, retina defects, cystic kidneys, lung or airway defect, hydrocephalus, diabetes and obesity[65,66].

Primary cilia are typically 1-15µm long. There are 3 components in the primary cilia structure: basal body, transition zone, and the axoneme (Figure 2). The basal body originates from a mother centriole that is anchored to the cell membrane via transition fibers. The basal body is the nucleation site for the growth of axoneme microtubules. In between the basal body and the axoneme lies the transition zone. The transition zone is characterized by Y-shaped connectors between axoneme microtubule doublets and the ciliary membrane; and forms a diffusion barrier for membrane soluble proteins. In contrast to motile cilia whose axoneme has 9 microtubule doublets with 2 single central microtubules (9+2), primary cilia just have 9 microtubule doublets (9+0). The lipid and protein composition of primary cilia are distinct from that of the plasma membrane[65]. The periciliary membrane is invaginated and dubbed the ciliary pocket, which has a lot of clatherin coated pits which make it a hotspot for endo- and exo-cytosis. The intraflagellar transport (IFT) complex facilitate the transport of cargo proteins along the primary cilium: IFT-B is responsible for anterograde transport (to ciliary tip), and IFT-A is responsible for retrograde transport (to ciliary base). IFT-B complex transports proteins into the cilium. The BBSome is necessary for the exit of activated GPCRs out of the cilium[67].

Ciliopathies with obesity as a clinical feature

Bardet-Biedl syndrome (BBS) is characterized by pediatric obesity, type 2 diabetes, mental impairment, polydactyly, retinitis pigmentosa, and kidney abnormalities. BBS is associated with mutations in the 28 identified BBS genes. Mutations in some BBS genes are more highly associated with obesity than others[68]. Eight *BBS* gene products (BBS1, BBS2, BBS4, BBS5, BBS7, BBS8, BBS9, BBS18) form a stable complex called the BBSome, which is required for the trafficking of signaling receptors and structural proteins along the primary cilium[68,69]. BBS6, BBS10, and BBS12 form a chaperonin like protein complex that regulates BBSome assembly and downstream ciliary signaling[53,70]. The role of the remaining BBSome proteins still needs to be fully elucidated. Genetic defects in BBSome proteins compromise the function of cilia resulting in defects in ciliary

signaling or ciliary protein trafficking. Most *Bbs* mouse models (except *Bbs3*) exhibit hyperphagia induced obesity and several other clinical features of BBS patients with varying penetrance and expressivity[71].

Patients with Alström (ALMS) syndrome have obesity, type 2 diabetes, rod-cone dystrophy, cardiomyopathy, male infertility, hearing loss, fibrosis and multiple organ failure[71,72]. Alstrom syndrome is associated with mutations in a single gene, *ALMS1*. ALMS1 protein localizes to the base of the cilium and has a role in cilia formation and stability. Most human ALMS1 mutations lead to a truncated protein that does not affect ciliogenesis however proper cilia function and cilia maintenance are affected[69]. Mouse models for ALMS1 (the fat aussie/*Alms1*$^{foz/foz}$; gene trapped/*Alms1*$^{-/-}$; and *Alms1*$^{flin/flin}$) exhibit most of the clinical features found in ALMS patients[73,74]. In the fat aussie mouse, which has a mutation in Alms1 that results in a truncated ALMS1 protein, ALMS1 fails to localize to the cilium which leads to fewer ciliated neurons in the hypothalamus[69,71].

Other ciliopathies associated with obesity include MORM, and Carpenter syndromes. MORM (Mental retardation, truncal Obesity, Retinal dystrophy, and Micropenis) syndrome is caused by mutations in the inositol polyphosphate-5-phosphatase E (*INPP5e*). INPP5E forms and maintains the unique ciliary membrane lipid composition (rich in PI(4)P) which is essential for ciliary signaling[64]. ARL13B (an ADP-ribosylation factor protein family member) is involved in the retention of INPP5E in the primary cilium[75,76]. Mutations affecting the ability of INPP5E to localize to the primary cilium cause MORM[76]. Interestingly, a recent study demonstrated that mutations that prevent ARL13B localization to the primary cilium, but leave its GEF activity intact, cause obesity[77]. Symptoms of Carpenter Syndrome include: obesity, crainiosynostosis, and soft tissue syndactyly. It results from mutations in the *RAB23* gene. RAB23 is a small GTPase which transports receptors to cilia[64,69].

Other ciliary genes associated with obesity

Mutations in these genes are also linked with monogenic obesity: Centrosomal protein 19 (*CEP19*, protein product localizes to the basal body and plays a role in ciliary protein trafficking), and ANKH (*ANKH*, is a transmembrane protein that localizes to the basal body)[64].

Retinitis pigmentosa GTPase regulator-interacting protein-1 link (*RPGRIP1L*) codes for a protein that localizes to the Y linkers of the transition zone. It was first identified as a gene close to the FTO locus, which has the GWAS SNP with the highest association to obesity in its intron. Because this SNP is located in the first intron of the FTO gene, it is difficult to pinpoint the exact link between this SNP and obesity. It has been demonstrated that this SNP alters a regulatory element recognized by the transcription factor, CUX1, which leads to decreased expression of FTO and RPGRIP1L. Subsequent experiments showed that Rpgrip1l knock out mice develop obesity and that RPGRIP1L mediates the transport of LEPR to the periciliary area[21].

Mutations in tubby gene (*Tub*) causes retinal degeneration, hearing loss, and late-onset obesity. The tubby gene family includes tubby, and tubby-like proteins 1, 2, and 3 (TULP1-3). Interestingly, mutations in TULP do not cause obesity[78]. Tub and TULP3 are responsible for GPCR trafficking into the ciliary membrane[79,80].

Neuronal Communication: Synaptic vs Volumetric

Neuronal communication is canonically known to happen within small gaps called synapses (synaptic transmission). This process involves the activation of the presynaptic neuron which results in the release of neurotransmitter at the presynaptic bouton. The neurotransmitter then diffuses through the synaptic cleft (tens of nanometers across) and binds to receptors on the postsynaptic surface. Synaptic transmission between 2 neurons is rapid, and specific (Figure 3)[81].

In the 1980s, the idea of volume transmission was introduced[82]. Volume transmission occurs when a neuron releases neuromodulators into the extracellular space, and the neuromodulators can diffuse across hundreds of nanometers or millimeters to bind to its receptor on the target neuron (Figure 3)[81,83]. Volumetric transmission can act on many different neurons, cell types and regions; and allows for long lasting modulatory effects. The distance in which a neuromodulator can travel depends on its energy gradients, extracellular space morphology, and clearance rate. There are many requirements for volumetric transmission to occur: neurotransmitter can be released into the extracellular space (via extrasynaptic exocytosis for example); extrasynaptic receptors on target cells (for example, receptors on primary cilia); sufficient amount of neurotransmitter reaches these receptors; presence of a mechanism to degrade the neurotransmitter outside of the synapse[81]. Volumetric transmission is slower and affects a broader area than synaptic transmission.

In current models, the encoding of information by neurons is based on synaptic transmission. It involves the presentation of a novel stimulus which causes the activation and synaptic firing of certain neurons. Repeated presentation of this stimulus causes consolidation of the memory at the cellular and molecular level in the synapse. While short term memories involve increases in presynaptic neurotransmitter release and postsynaptic receptor localization, long term memories involve changes in transcription which ultimately results in synaptic growth or neuron excitability[84,85]. The field of long-term information encoding has focused on storage of memories via changes in synaptic transmission, however, whether other cell types in the brain are involved in encoding or storage and if all information is stored via changes in synaptic transmission is unknown. Because neuronal communication can also occur via neuromodulators that are extrasynaptically released and bind to extrasynaptic receptors on neurons and other cell types, it is unknown whether changes in volumetric signaling or changes as a result of volumetric signaling can also store information.

Figures

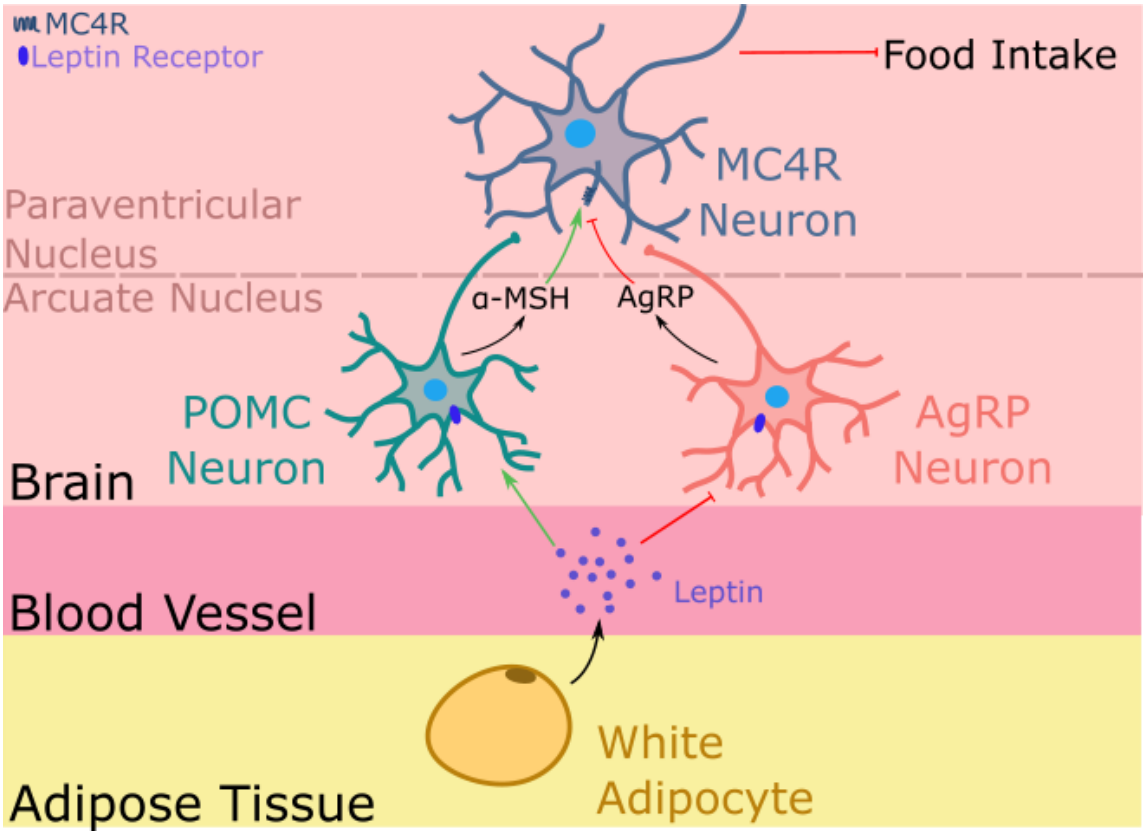


Figure 0.1 The leptin melanocortin pathway.

White adipocytes release leptin into the circulation which activates POMC neurons. Activated POMC neurons will release αMSH which binds and activates MC4R. Once MC4R is activated, food intake is inhibited. Leptin inhibits AGRP neurons. When there are low levels of leptin in the circulation, AGRP neurons are activated and secrete AGRP which inhibits MC4R thus leading to food intake.

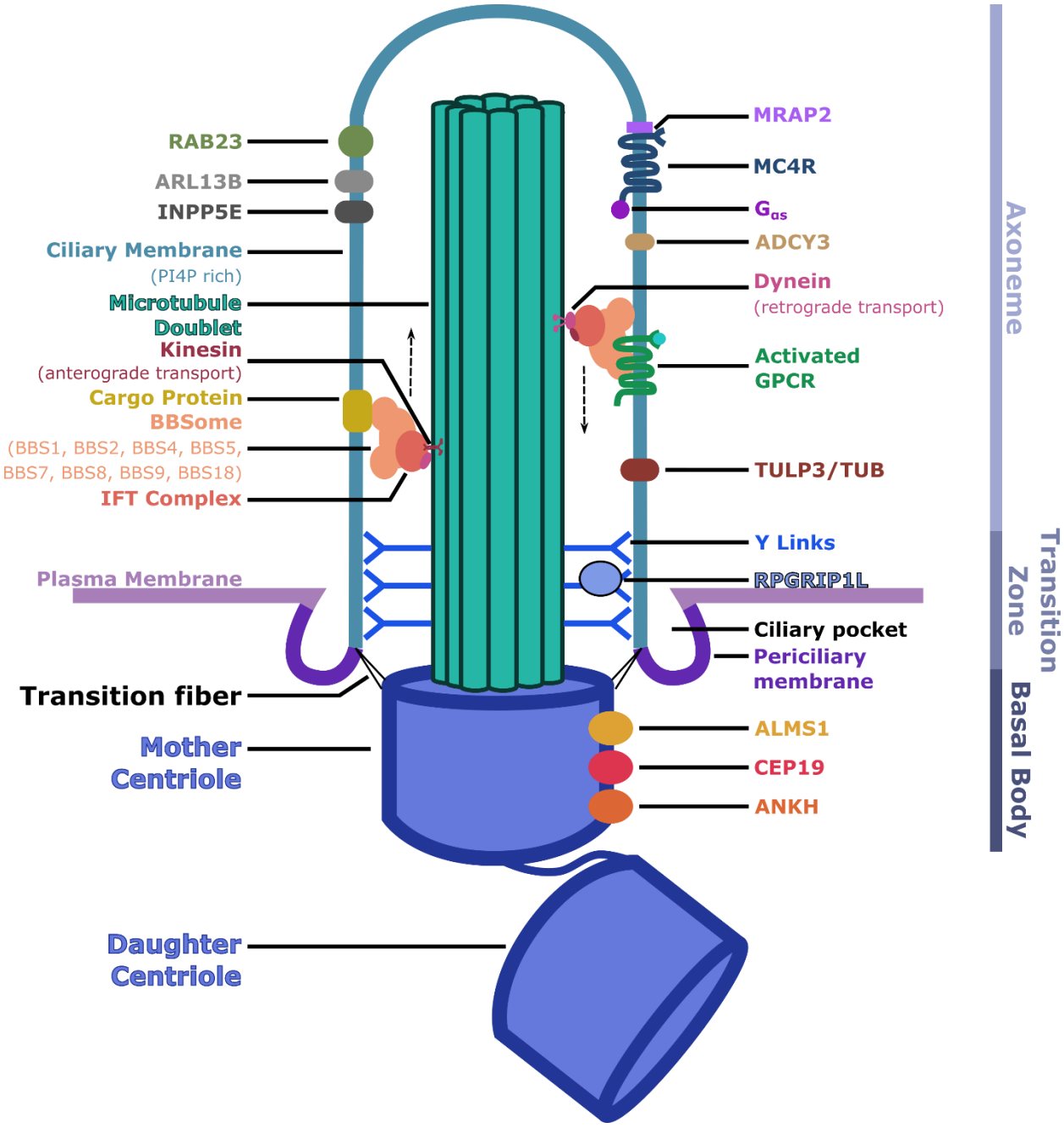


Figure 0.2 Primary cilia structure and components

Primary cilia is an organelle that protrudes out of the cell's plasma membrane. It is made up of 3 different structures: basal body, transition zone, axoneme.

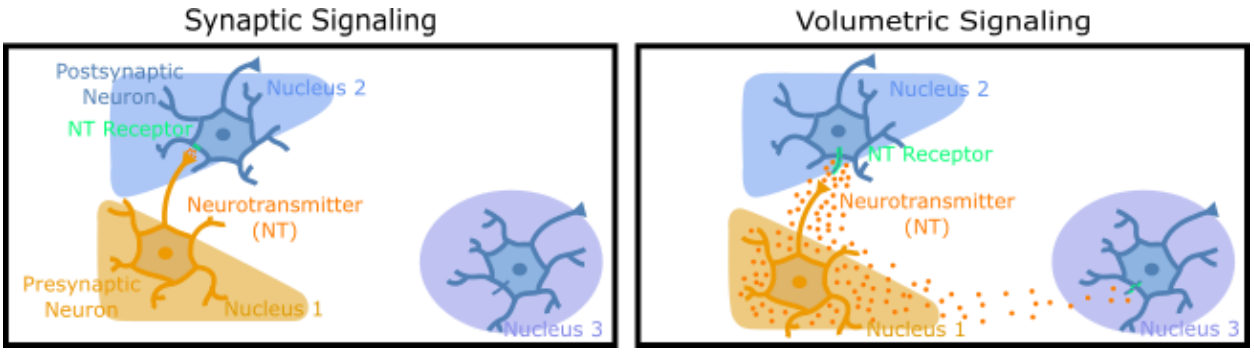


Figure 0.3 Synaptic vs volumetric signaling.

Synaptic signaling occurs between 2 neurons: the presynaptic neuron releases neurotransmitter into the synaptic cleft which binds to neurotransmitter on the postsynaptic neuron. Volumetric signaling can result in signaling to multiple neurons in multiple locations in the brain.

Transition

How neurons encode energy homeostasis is unknown. Previous works have demonstrated that MC4R on MC4R neurons in the PVN integrate orexigenic and anorexigenic signals, and signals satiety. More recently, we have demonstrated the importance of MC4R localization and signal at the primary cilium of MC4R neurons. In the next chapter, I will validate genetic mouse models made to facilitate studies on MC4R neurons. The subsequent chapter, I will present evidence for neuronal encoding of energy homeostasis through localization of MC4R at the primary cilium.

Chapter 1: Characterization of mouse models

Summary

MC4R is integral to the maintenance of energy balance as MC4R neurons integrate information from the rest of the leptin melanocortin pathway; it is the second highest obesity associated gene in GWAS studies; and mutations in MC4R is the leading cause of monogenic obesity. Studying MC4R in the brain is challenging because MC4R is expressed in very few neurons across the brain, MC4R is expressed in low levels, and there is no commercially available antibody against MC4R. We have generated two different mouse lines to tackle these problems: *Mc4r-t2a-Cre* and *Mc4r-eGfp* mouse lines. Here we validate both these mouse lines.

Introduction

Mutations in melanocortin 4 receptor (MC4R) is the most common cause of monogenic, severe, early-onset obesity, thus the proper function of MC4R is crucial for the maintenance of energy homeostasis. MC4R is a seven transmembrane G-protein coupled receptor (GPCR). It is part of the leptin melanocortin pathway, which maintains long term energy homeostasis by integrating orexigenic and anorexigenic signals from the periphery and the first order neurons of this pathway[52]. Activation of MC4R results in the activation of adenylyl cyclase and increase in cyclic adenosine monophosphate (cAMP) levels, which ultimately leads to the inhibition of food intake[86,87].

There are many challenges involved in studying MC4R and MC4R neurons *in vivo*. First, MC4R neurons are small subpopulations of neurons in nuclei throughout the brain. Second, the MC4R protein is difficult to detect because of low expression levels and the lack of working antibodies[54]. Thus, genetic manipulations of MC4R neurons to study MC4R neuron function, and examining MC4R subcellular localization or trafficking is difficult.

We have generated two different mouse lines to aid in the studying of MC4R neurons: the *Mc4r-t2A-Cre* mouse line and the *Mc4r-eGfp* mouse line. Here we validate the two different MC4R mouse models.

Results

Generation and Validation of *Mc4r-t2A-Cre* mice

We generated an $Mc4r^{t2aCre}$ allele via CRISPR/Cas9-mediated zygotic recombination. We inserted the T2A sequence followed by a Cre recombinase open reading frame at the terminator codon of *Mc4r* so that the endogenous promoter/enhancer elements direct Cre expression to MC4R-expressing cells (Figure 1a). Expression of this locus will result in a MC4R-T2A-Cre fusion protein which will be self-cleaved at the T2A sequence, thus Cre can be trafficked into the nucleus and MC4R subcellular localization is not affected. Accurate insertion at the *Mc4r* locus was verified by long-range PCR and sequencing. Recombinase activity, assessed in $Mc4r^{t2aCre/t2aCre}$ $Rosa26^{Ai75/Ai75}$ mice which express a red fluorescent protein in a Cre-dependent fashion, recapitulated the endogenous MC4R expression in particular in the PVN (Figure 1c, 1d). Importantly, the weight curves of mice homozygous for the insertion ($Mc4r^{t2aCre/t2aCre}$) did not differ from those of WT littermates. This allele will allow us to manipulate MC4R neurons in specific nuclei of the brain.

Generation and Validation of *Mc4r-eGfp* mice

We also generated an $Mc4r^{eGfp}$ allele in the same manner as the *Mc4r-t2a-Cre* allele. In this case, we inserted an eGFP tag at the C terminus of MC4R (Figure 2a). We verified that PVN^{MC4R} neurons also expressed eGFP; and that only PVN^{MC4R} neurons expressed eGFP using RNAScope (Figure 2b).

Assessing MC4R and MRAP2 colocalization throughout the brain

Using this allele, we assessed MC4R colocalization with MRAP2 at the primary cilium. We have previously demonstrated that MRAP2 localizes to the neuronal primary cilium and MRAP2 is necessary for MC4R localization at the primary cilium; and PVN^{MC4R} colocalizes with MRAP2 at the primary cilium. We sought to determine whether MC4R colocalizes with MRAP2 at the cilium in other brain regions with MC4R expression. We found that, although MRAP2 expression is broader than MC4R's, MC4R always colocalizes with MRAP2 at the primary cilium in other nuclei where MC4R is expressed (Figure 3). We also demonstrate that MC4R localizes to the primary cilium in nuclei outside of the PVN; and that MC4R-GFP is expressed in all nuclei that have been reported to express MC4R.

Discussion

In this chapter, we have validated two knock-in mouse lines. We have demonstrated that Cre has been successfully inserted into the Mc4r locus of the Mc4r-t2a-Cre mouse line and is expressed at sufficient levels to cause germline recombination; and does not affect body weight. We have also demonstrated that Gfp has been inserted into the Mc4r locus of the Mc4r-eGfp mouse line by showing that neurons that express Mc4r also express eGfp.

These mouse lines will help us address questions regarding MC4R neuronal subpopulations in different regions of the brain by allowing us to inject adenoassociated viruses (AAV) to introduce cre dependent proteins into specific locations of the brain

The *Mc4r-t2a-Cre* mouse line will allow for specific manipulation of MC4R neuronal subpopulations in different regions of the brain through use of Cre dependent protein expression. These techniques include crossing *Mc4r-t2a-Cre* mice to mice with floxed alleles to cause germinal expression or deletion of proteins; injecting Cre dependent viruses into the lateral ventricle in P0 pups to induce expression of proteins in all MC4R neurons across the brain; or by stereotaxically injecting Cre dependent viruses into specific nuclei of adult mice. The cre-lox system is a common method of inducing gene expression in/manipulating specific cell populations, thus there is a large toolbox available for use in *Mc4r-t2a-Cre* mice. Having a Cre expression specifically in MC4R neurons would allow us to have temporal and regional control genetic and cellular manipulations thus allowing us to study molecular and cellular functions of MC4R neurons in energy homeostasis.

The *Mc4r-Gfp* allele allows us to assess MC4R localization which previously could not be done *in vivo* as there are no commercially available antibodies against MC4R. To address the low levels of *Mc4r* expression thus low levels of MC4R-GFP fluorescence, we can stain for GFP tag to amplify the GFP signal. Using the *Mc4r-Gfp* allele, we have demonstrated that MC4R colocalizes with ADCY3, thus MC4R goes to the neuronal primary cilium in the PVN[54] and in other regions of the brain. We have also demonstrated that MC4R colocalizes with MRAP2 at neuronal primary cilium

and that MRAP2 is necessary for MC4R localization to the primary cilium using the *Mc4r-Gfp* allele[63]. The *Mc4r-Gfp* allele will allow us to study MC4R protein trafficking *in vivo* under physiological conditions, MC4R interactions with other proteins, and the effects of other proteins on MC4R localization.

Figures

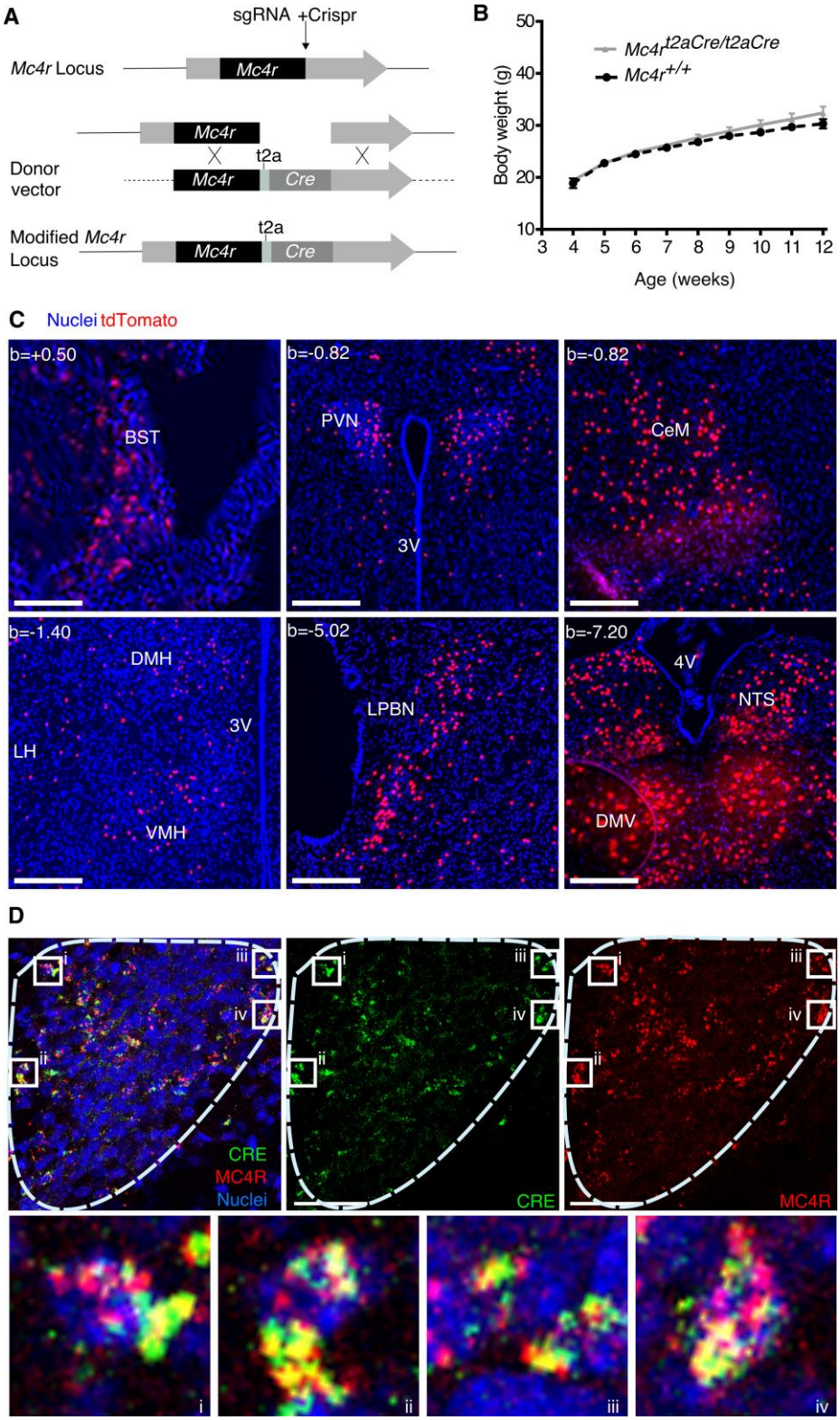

A
sgRNA +Crispr
Mc4r Locus
Mc4r
Donor vector
t2a
Cre
Modified Mc4r Locus
B
Mc4r t2aCre/t2aCre
Mc4r +/+
Body weight (g)
Age (weeks)
C
Nuclei tdTomato
b=+0.50
BST
b=-0.82
PVN
3V
b=-0.82
CeM
b=-1.40
DMH
3V
LH
VMH
b=-5.02
LPBN
b=-7.20
4V
NTS
DMV
D
i
ii
iii
iv
CRE
MC4R
Nuclei
CRE
MC4R

Figure 1.1 Characterization and validation of Mc4r-t2a-Cre allele.

(A) Strategy used to target the mouse *Mc4r* locus by CRISPR/Cas9 to insert a *T2A* and *Cre* open reading frame in frame with *Mc4r*.

(B) Body weights of $Mc4r^{t2aCre/t2aCre}$ (n=7) mice and their $Mc4r^{+/+}$ littermates (n=6).

(C) The expression of the *Mc4r-t2a-Cre* allele was surveyed in the brain of an $Mc4r^{t2aCre/t2aCre}$ $Rosa^{Ai75}$ mouse on the rostral-caudal axis. Scale bar, 250µm.

(D) *Mc4r* (red) and *Cre* (green) mRNA transcripts in the PVN of a $Mc4r^{t2aCre/t2aCre}$ P6 mouse pup, detected using RNAScope Multiplex Fluorescent V2 Assay, colocalize in the same cells. Each punctum represents one mRNA transcript. Scale bar, 50µm. BST, bed nucleus of the stria terminalis; CeM, central amygdaloid nucleus; DMH, dorsal medial hypothalamus; DMV, dorsal motor nucleus; LH, lateral hypothalamus; LPBN, lateral parabrachial nucleus; PVN, paraventricular nucleus; NTS, nucleus of the solitary tract; VMH, ventromedial hypothalamus.

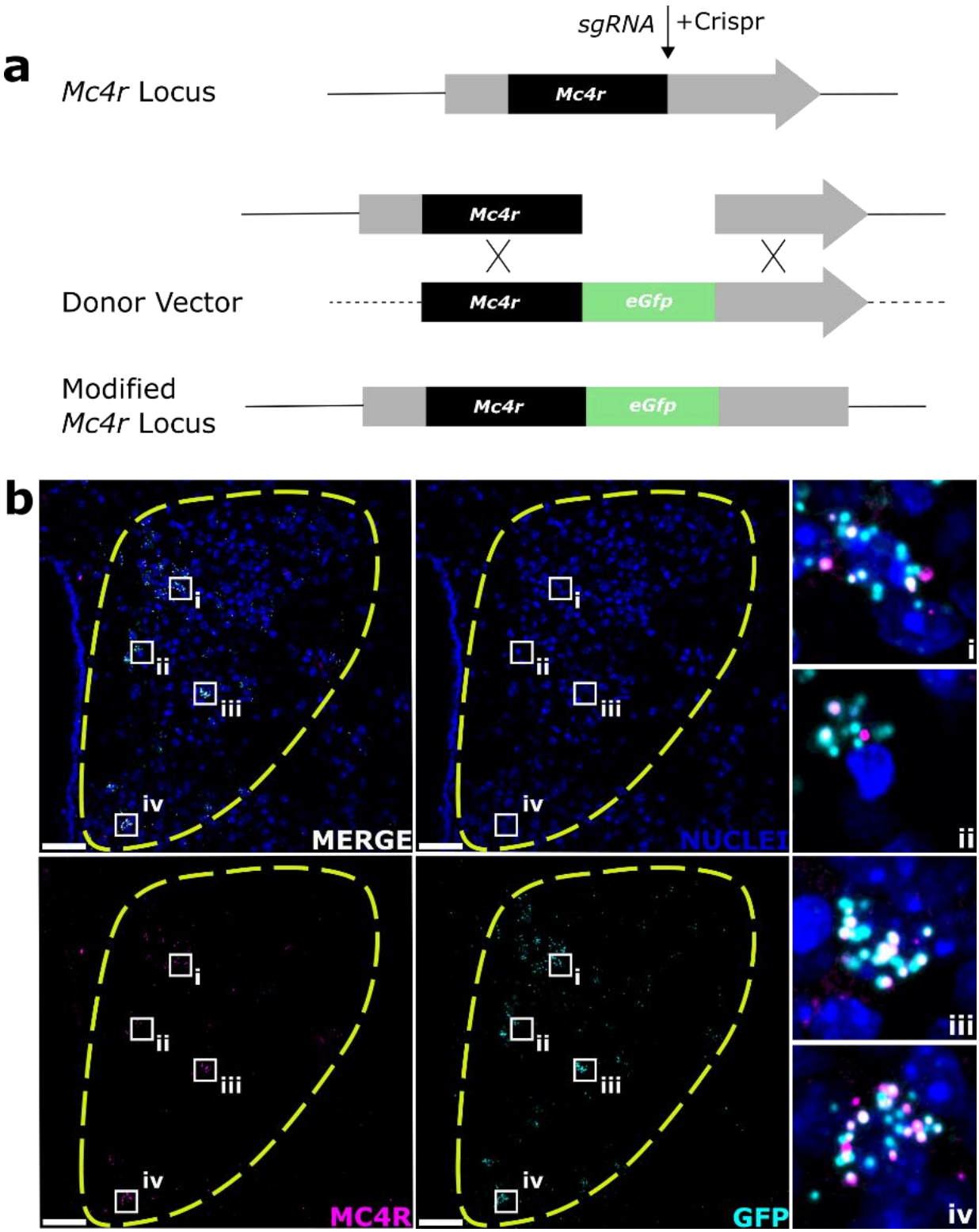

a
Mc4r Locus
sgRNA
+Crispr
Mc4r
Donor Vector
Mc4r
eGfp
Modified
Mc4r Locus
Mc4r
eGfp
b
i
ii
iii
iv
MERGE
NUCLEI
MC4R
GFP

Figure 1.2 Mc4r-eGfp allele design and verification.

(A) strategy used to target the mouse *Mc4r* locus by CRISPR/Cas9 to insert an *eGFP* open reading frame in frame with *Mc4r*.

(B) *Mc4r* (magenta) and *eGfp* (cyan) mRNA transcripts in the PVN of $Mc4r^{Gfp/Gfp}$ 4-week mouse, detected using RNAScope Multiplex Fluorescent V2 Assay, colocalize in the same cells. Each punctum represents one mRNA transcript.

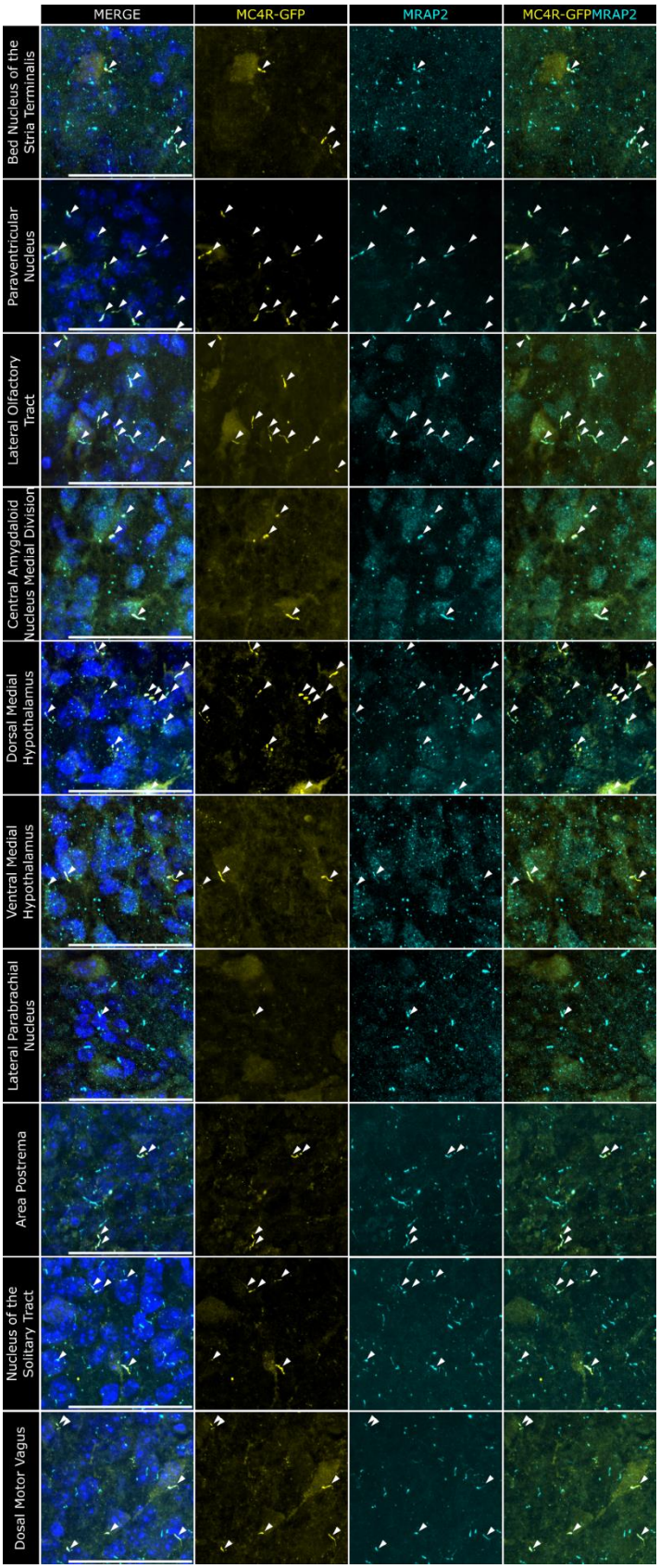

MERGE
MC4R-GFP
MRAP2
MC4R-GFPMRAP2
Bed Nucleus of the Stria Terminalis
Paraventricular Nucleus
Lateral Olfactory Tract
Central Amygdaloid Nucleus Medial Division
Dorsal Medial Hypothalamus
Ventral Medial Hypothalamus
Lateral Parabrachial Nucleus
Area Postrema
Nucleus of the Solitary Tract
Dosal Motor Vagus

Figure 1.3 MC4R colocalization with MRAP2 at neuronal primary cilium in select nuclei.

Immunofluorescence imaging showing co-localization of MC4R-GFP (yellow) with MRAP2 (cyan) at the neuronal primary cilium. Nuclei are shown in blue. Primary cilium double positive for MC4R-GFP and MRAP2 are indicated by arrows. Scale bar:50µm

Methods

Animals

Mice were housed (with enrichment) in a barrier facility and maintained on a 12-hour light/12-hour dark cycle (on: 0700–1900 hours) at an ambient temperature of 23°C ± 2°C and relative humidity at 50%–70%. Mice were fed a rodent 5058 diet (LabDiet) and group housed (up to 5 mice per cage) or single housed after surgery. Experiments were performed using weight- and sex-matched littermates. Mouse alleles used are: *Rosa*^{Ai75} (*Gt(ROSA)26Sor*$^{tm14(CAG-tdTomato)Hze}$), *Mc4r*$^{tm2(t2a\ Cre)Vai}$, and *Mc4r*$^{tm1(egfp)Vai}$.

Generation of knock-in mice

The generation of knock-in mice was performed at the Gladstone Institute mouse transgenic core. Briefly, Superovulated female FVB/N mice (4 weeks old) were mated with FVB/N stud males. Fertilized zygotes were collected from oviducts and injected with (a) Cas9 protein (50 ng/μL), (b) a donor vector (20 ng/μL) consisting of 1 kb of the 5′ flanking sequence (i.e., the MC4R coding sequence) followed by t2aCre and 5.5 kb of the 3′ flanking sequence; or by Gfp (cloned into frame) and 5.5kb of the 3′ flanking sequence, and (c) a sgRNA (25 ng/μL), of which the guide sequence (5′-GTCTAGCAGGTATTAAGTGG-3′ for *Mc4r-t2a-Cre* and 5′- GTCTAGCAGGTATTAAGTGGGGG-3′ for *Mc4r-eGfp*) was designed to target nucleotides immediately downstream of the MC4R stop codon in a short region that was not present in the donor vector injected into the pronucleus. Injected zygotes were implanted into oviducts of pseudopregnant CD1 female mice. Pups were genotyped for insertions at the correct loci by PCR. MC4R neuron–specific expression of Cre in the *Mc4r-t2a-Cre* mouse was verified by crossing mice with *Gt(ROSA)26Sor*$^{tm14(CAG-tdTomato)Hze}$ mice and through RNAScope; and in the *Mc4r-eGfp* mice through RNAScope and confocal imaging in nuclei throughout the brain that have been reported to have Mc4r expression. One entire mouse brain (coronal sections) was imaged and analyzed to assess Cre expression throughout the brain. One entire P6 pup brain (coronal sections) was imaged and analyzed to assess Gfp expression throughout the brain.

Direct fluorescence and immunofluorescence studies of mouse brain

Mice were perfused transcardially with PBS followed by 4% paraformaldehyde fixation solution. Brains were dissected and postfixed in fixation solution at 4°C overnight, soaked in 30% sucrose solution overnight, embedded in O.C.T. (Tissue-Tek, Sakura Finetek USA), frozen, and then cut into 20–35 μm coronal sections and stored at –80°C until use for staining.

After washing, sections were blocked for 1 hour in 50% serum, 50% antibody buffer (1.125% NaCl, 0.75% Tris base, 1% BSA, 1.8% l-lysine, 0.04% azide), followed by incubation with primary antibodies overnight at 4°C. After washing, the sections were incubated with secondary

antibodies for 1 hour at room temperature, washed and stained with Hoechst (1:5000), and then washed and mounted with ProLong Diamond Antifade Mountant (Thermo Fisher Scientific).

The following primary antibodies were used: chicken anti-GFP (Abcam, ab13970, 1:250); rabbit anti-MRAP2, Proteintech, 17259-1-AP, 1:200.

The following secondary antibodies were used: goat anti–chicken Alexa Fluor 488 (Invitrogen, Thermo Fisher Scientific, A11039), 1:500; goat anti–rabbit Alexa Fluor 633.

RNAScope

To detect single mRNA molecules, RNAScope (Advanced Cell Diagnostics [ACD]) was performed on 20 µm frozen hypothalamic sections from a P6 *Mc4r*$^{t2aCre/t2aCre}$ pup brain prepared as described above. The RNAScope Fluorescent Multiplex Kit V2 (catalog 323100) was used according to the manufacturer's instructions. Briefly, slides were dried at –20°C for 1 hour and then at –60°C for 30 minutes. Next, they were postfixed in 4% paraformaldehyde before being dehydrated in 50%, 70%, and 100% ethanol for 5 minutes. After letting the slides dry for 5 minutes at room temperature, hydrogen peroxide was added to the slides for 8 minutes. Target retrieval was performed in a steamer at 100°C. Slides were first equilibrated to the steamer in distilled water and then placed in ACD's 1× target retrieval agent. Slides were then allowed to dry overnight. The next day, the slides were treated with protease III for 10 minutes at room temperature. *Cre-C2* (*ACD*, *312281-C2*) and *Mc4r-C3* (*ACD*, *319181-C3*) probes were diluted at a 1:50 ratio with probe diluent (ACD, 300041) and incubated on the slides for 2 hours at 40°C, followed by 3 amplification steps. Opal 520 (Akoya Biosciences, FP1487001KT) and Opal 570 (Akoya Biosciences, FP148800KT) fluorophores were diluted 1:1500 in TSA buffer. The Cre-C2 probe was developed with Opal 520 Fluorophore, and the Mc4r-C3 probe was developed with Opal 570 Fluorophore. DAPI was added to label the nuclei, and slides were mounted with ProLong Gold (Thermo Fisher Scientific).

Image capture and processing

Images of *Mc4r*$^{t2aCre/t2aCre}$ *Rosa*^{Ai75} brain was captured using the Keyence BZ-X710. RNAScope images were acquired with a Leica SP8 confocal microscope. Confocal images of MC4R-GFP and MRAP2 were captured using Nikon CSU-W1/SoRa spinning disk confocal.

Images were processed with Fiji software (ImageJ, NIH). Maximal intensity Z projections are from at least 20 slices over 10–20 µm in size.

Transition

In this chapter we presented and validated 2 different mouse lines that allowed us to study MC4R localization and MC4R neuron function.

Using the *Mc4r-eGfp* allele, we have demonstrated that MC4R localization at the primary cilium is dynamic throughout murine developmental stages: most concentrated at the primary cilium in young pups but gradually leaves the primary cilium at 2weeks old to adulthood[57]. In the next chapter, we will use the *Mc4r-eGfp* mouse line for assessing changes in MC4R localization under different feeding states as MC4R is involved in food intake and energy balance control.

Chapter 2: Molecular encoding of peripheral energy levels by neuronal cilia

Xinyu Yue[*], Adelaide Bernard[*], Francois Mifsud[*], Irene Ojeda-Naharros, Zhixuan Zhang, Coralie Alexandre, Abbey Diener Blake, Aristides G. Diamant, Marine Benois, Alicja Bednarska, Kellan Kim, Erin McDaid, Sumei Zhang, Nicolas F. Berbari, Jeremy F. Reiter[3,5,6], Maxence V. Nachury, Christian Vaisse

Summary

How the brain encodes information at the molecular level is a central question in neuroscience. We find that neurons can encode information through changes in ciliary composition. Specifically, we report that the dynamic trafficking of melanocortin 4 receptor (MC4R) to and from neuronal primary cilia is responsible for storing information on peripheral energy levels. MC4R is a ciliary G_s coupled G protein coupled receptor; and disruption of its localization or signaling at neuronal primary cilium leads to hyperphagia and obesity. We demonstrate that MC4R protein accumulates at the primary cilium during energy deficit, and ciliary accumulation of MC4R is inversely proportional to levels of circulating leptin, a hormone produced by adipocytes in proportion to peripheral energy stores. Mechanistically, MC4R localization depends on levels of its inverse agonist, AGRP, which is regulated by leptin. With increasing levels of energy deficit, MC4R accumulation at cilia propagates to further brain regions. We propose that MC4R localization is the molecular and cellular basis for integrating information on peripheral energy stores, and novel method for encoding long-term energy homeostasis. These findings also reveal that neurons can encode and store information via changes in ciliary composition.

Introduction

To maintain energy balance, the central nervous system controls feeding in response to leptin, a hormone secreted by adipocytes in proportion to fat stores. Decreased leptin levels engage neurons of the hypothalamic melanocortin system to coordinate increased food intake and replenishment of energy stores[88–91]. In the hypothalamus, GABAergic orexigenic AGRP neurons release hunger-promoting agouti-related peptide (AGRP) and neuropeptide Y (NPY). Glutamatergic anorexigenic POMC neurons release the satiety-promoting α-Melanocyte-Stimulating Hormone (αMSH)[92,93]. Both AGRP- and αMSH-producing neurons communicate to neurons expressing the receptor for αMSH and AGRP, the melanocortin-4 receptor (MC4R)[88–90,94,95].

The hypothalamic melanocortin system integrates and responds to immediate changes in nutritional availability to modulate hunger at short-time scales[96,97]. Recent work has focused on the activity modulation and response integration of these neurons at these short-time scales through synaptic signaling[96,98,99]. In particular, the activity of AGRP-producing neurons is rapidly modulated by sensory[98] and interoceptive[99,100] detection of food, affecting downstream second order neurons, including MC4R-expressing neurons, through GABAergic synapses[101–103].

Over the longer term, the hypothalamic melanocortin system also matches food intake to energy expenditure by processing and integrating information about energy balance. In the first order ARC neurons, the leptin receptor engages the cytokine-like Jak-Stat signaling pathway to control the secretion of aMSH and AGRP[92,93,104–107]. Whether and how second order MC4R-expressing neurons interpret these leptin-regulated, longer-term homeostatic inputs differently from the short-term inputs is unknown.

We have recently demonstrated that MC4R localizes to the primary cilia of neurons and that the cilia of PVN^{MC4R} neurons are required for MC4R control of food intake. Primary cilia are specialized sensory organelles projecting from the cell body which detect diverse signals[78,108–112]. The primary cilia membrane's composition is actively regulated and distinct from that of the plasma membrane, allowing for distinct signaling in each compartment[112]. Importantly, the ciliary localization of certain receptors, and thus their capacity to signal, can be modulated by their ligands. For example, the ciliary Hedgehog receptor PTCH1 is removed from the cilium upon binding Hedgehog ligand[112,113].

Here we show that MC4R subcellular localization to the primary cilium is dynamic, regulated and correlates with physiological levels of energy deficit. Specifically, MC4R localization to the primary cilia is inversely proportional to circulating leptin levels and fat stores, and decreased leptin levels enrich MC4R at the primary cilium. Mechanistically, this enrichment at the primary cilium is dependent on the inverse agonist AGRP. These findings provide a substrate for the longer-time scale representation of energy deficit within the brain and provides a molecular and cellular explanation for the biasing of the melanocortin system towards feeding[39,114].

Results

Fasting leads to accumulation of MC4R at primary cilia.

To determine whether MC4R subcellular localization is impacted by physiological changes, we compared ciliary localization of MC4R-GFP in the PVN of *Mc4r*$^{Gfp/Gfp}$ mice fasted for 24hr to that of ad lib fed mice. In fasted mice, there was an apparent increase in both the number of neuronal primary cilia at which MC4R was detected, as well as an increase in the amount of MC4R detected in these cilia (Figure 1a).

To quantitate ciliary localization across the entire PVN, we established a workflow involving the identification of neuronal primary cilia and MC4R-GFP positive cilia (Figure 1b, S1, S2 and methods). Specifically, we immunostained sections from the anterior (Bregma=0.7mm), middle (Bregma=0.82mm), and posterior (Bregma=0.94mm) regions of the PVN for the basal body component CEP43, the neuronal cilia component ADCY3, and MC4R-GFP (Figure 1a). Sections are imaged at 60x magnification using a confocal microscope to obtain z-stacks images of the PVN. We trained two independent AI models to identify neuronal primary cilia and MC4R-GFP positive cilia, respectively (Figure S2a, S2b), enabling the calculation of the proportion of neuronal cilia at which MC4R-GFP was detected (Figure 1c) and of the enrichment of MC4R-GFP at these cilia (Figure 1d).

This quantification revealed that a 24hr fast leads to a 10-fold increase in the number of PVN cilia at which MC4R-GFP is detected (Figure 1c) and to a significant increase in the amount of MC4R-GFP at PVN cilia (Figure 1d). These increases were observed in both male and female mice fasted for 24h.

MC4R localization to primary cilia of PVN^{MC4R} neurons correlates with energy deficit

Calorie restriction induces numerous changes at different time scales in neurons of the melanocortin pathway. We further determined the dynamic of MC4R accumulation at cilia by evaluating its levels in mice under increasing levels of energy deficit. Specifically, MC4R levels in PVN^{MC4R} neuronal cilia were assessed in mice fasted for 12, 24 or 48 hours, or placed on 30% calorie restriction for 10 days (Figure 2a, S3). We find that the maximal number of neuronal primary cilia at which MC4R is detected is reached after a 12hr fast but that MC4R continues to gradually accumulates at these cilia with increased length of fasting (Figure 2b-d). To determine to what extent MC4R accumulation at primary cilia is related to long-term energy storage, we examined the relationship between the level of accumulation of MC4R at PVN^{MC4R} neuronal cilia and the level of energy deficit as measured by decrease in fat mass and leptin levels in the calorie restricted mice. We find that MC4R ciliary levels, as measured by our assay, are closely correlated with both these variables (Figure 2e, 2f, S4). These results demonstrate that changes in MC4R localization are progressive, cumulative and occur at longer time scale than changes in

neuronal activity in response to food cues. These results also indicate that MC4R localization to primary cilia of PVN^{MC4R} neurons correlates with energy deficit and raise the question whether leptin regulates the amount of MC4R at cilia.

MC4R accumulation at PVN^{MC4R} neuronal cilia is leptin dependent

To assess whether leptin is necessary for MC4R accumulation at primary cilia, we quantified MC4R localization at primary cilium of PVN^{MC4R} neurons in leptin deficient *Lep$^{ob/ob}$ Mc4r$^{Gfp/Gfp}$* mice (Figure 3a). In the PVN of mice lacking leptin, the proportion of neuronal primary cilia harboring MC4R-GFP as compared to control (*Lep$^{+/ob}$ Mc4r$^{Gfp/Gfp}$* and *Lep$^{+/+}$ Mc4r$^{Gfp/Gfp}$*) littermates was dramatically increased (Figure 3a, 3b). Notably, the proportion of cilia at which MC4R was detected was similar to that of calorie restricted mice. Within MC4R positive cilia, MC4R fluorescence intensity was also higher in *Lep$^{ob/ob}$ Mc4r$^{Gfp/Gfp}$* mice compared to *Mc4r$^{Gfp/Gfp}$* mice (Figure 3a, 3c) and comparable to enrichment levels observed in fasted control littermate mice.

To further determine whether cilia subcellular localization of MC4R is leptin-dependent and whether it is reversible, we assessed whether leptin replacement affects MC4R ciliary localization. We infused leptin (10µg/day) in six-week-old *Lep$^{ob/ob}$ Mc4r$^{Gfp/Gfp}$* mice with subcutaneous osmotic pumps (Figure 3d). Leptin rescued the body weight of the leptin deficient mice (Figure S5) and reduced both the proportion of MC4R positive cilia and the amount of MC4R in these cilia to the level of that detected in the PVN (Figure 3e-g) of control mice. These results demonstrate that MC4R localization to primary cilia of PVN^{MC4R} neurons is dynamic, reversible and leptin-dependent.

AGRP is required for peripheral energy stores and leptin control of MC4R localization to cilia

A number of GPCRs exit cilia following ligand mediated activation of the receptor[115,116]. As decrease in leptin levels lead to increase production of AGRP, the inverse agonist of MC4R[102,117], we hypothesized that accumulation of MC4R at cilia depends on AGRP-mediated inhibition of MC4R activity. Therefore, we tested whether accumulation of MC4R at cilia requires AGRP.

We first investigated whether AGRP is required for the effect of calorie restriction on MC4R localization in *Agrp* null (*Agrp$^{-/-}$)* mice. Even in conditions of severe energy deficits in which MC4R accumulation at cilia of PVN^{MC4R} neurons was maximized (Figure 4a), ciliary localization of MC4R-GFP remained at the level of *ad lib* fed mice in *Agrp$^{-/-}$ Mc4r$^{Gfp/Gfp}$* mice demonstrating that AGRP is required for MC4R accumulation at cilia during calorie restriction (Figure 4b-d).

We also assessed whether AGRP was required for MC4R accumulation at PVN^{MC4R} neuronal cilia in leptin deficient mice. For this experiment we used the *Agrp^{Dtr}* allele in which the diphtheria toxin receptor **(**DTR) is targeted to the AGRP locus. As DTR is inserted at the start codon of AGRP, homozygous *Agrp$^{Dtr/Dtr}$* mice do not express AGRP[118]. We find that, in leptin and AGRP

deficient *Agrp*$^{Dtr/Dtr}$ *Lep*$^{ob/ob}$ *Mc4*$^{Gfp/Gfp}$ mice (hereby called *Agrp*$^{-/-}$ *Lep*$^{ob/ob}$ *Mc4r*$^{Gfp/Gfp}$ mice), levels of MC4R at cilia are reduced compared to *Lep*$^{ob/ob}$ *Mc4r*$^{Gfp/Gfp}$ mice (Figure 5a-c) and comparable to ciliary MC4R-GFP levels observed in *ad lib* fed mice. Thus, AGRP is required for MC4R-GFP accumulation at cilia in leptin deficient mice.

In heterozygous *Agrp*$^{Dtr/+}$ mice, AGRP is produced until injection of diphteria toxin (DT) which ablates AGRP neurons[24]. Ablation of AGRP neurons leads to inhibition of food intake, weight loss and death within 4-7 days due to loss of the tonic GABAergic activity of these neurons[24,118,119]. In leptin deficient *Agrp*$^{Dtr/+}$ *Lep*$^{ob/ob}$ mice, DT injection causes major weight loss but most animals survive[25]. We confirmed that ablation of AGRP neurons by injecting DT (1µg/mouse/day) in 14 week old leptin deficient *Agrp*$^{Dtr/+}$ *Lep*$^{ob/ob}$ *Mc4r*$^{Gfp/Gfp}$ mice resulted in weight loss (Figure 5d, S6).

We examined whether ablation of AGRP neurons also blocked the ability of leptin deficit to induce ciliary localization of MC4R-GFP. In the PVN of *Agrp*$^{Dtr/+}$ *Lep*$^{ob/ob}$ *Mc4r*$^{Gfp/Gfp}$ mice injected with DT, the number of MC4R-GFP positive cilia was decreased, as was the amount of MC4R-GFP at MC4R-GFP positive cilia (Figure 5e-g). These results demonstrate that ablation of AGRP neurons in adult mice is sufficient to decrease MC4R localization to the primary cilium in adult *Lep*$^{ob/ob}$ mice.

AGRP drives MC4R accumulation at primary cilia of PVN^{MC4R} neurons in adult mice

The demonstration that germ-line loss of AGRP or induced loss of AGRP neurons abrogates MC4R accumulation at cilia (Figure 4, 5a-c) suggested that AGRP is sufficient for promoting this accumulation. However, it does not exclude that this observation is the consequence of secondary developmental changes. In addition, decrease of ciliary MC4R after AGRP neuron deletion in adult mice also suggests that AGRP is sufficient to mediate this effect but does not exclude a role for NPY or GABA in promoting MC4R accumulation at cilia (Figure 5e-g).

To further determine whether AGRP is sufficient to promote MC4R accumulation at cilia, 7-week-old *Mc4r*$^{Gfp/Gfp}$ mice were infused with AGRP or artificial cerebrospinal fluid (aCSF, control) in the lateral ventricle for 10 days (Figure 6a). As previously reported, AGRP infusion increased body weight (Figure S7). In addition, AGRP infusion increased the proportion of MC4R-GFP positive cilia, and within MC4R-GFP positive cilia, the amount of MC4R-GFP at cilia (Figure 6b-d). These results demonstrate that AGRP is sufficient to accumulate MC4R at primary cilia in *ad lib* fed mice.

AGRP mediated increase in MC4R localization to primary cilia is cell autonomous

To demonstrate whether AgRP is required in a cell-autonomous manner for the accumulation of MC4R in the primary cilium, we employed an orthogonal *in vitro* approach. Mouse inner medulla collecting duct (IMCD3) cells stably expressing MRAP2 and MC4R-3xNeonGreen (hereafter MC4R^{3NG}) were used as a platform to provide unequivocal ciliary dynamic responses

to AgRP ligand. 24-hour incubation with 50 nM AgRP (10x EC50) increased ciliary MC4R by an average of 7-fold, thus recapitulating the ciliary MC4R increment observed *in vivo* (Figure 6 e, f).

Of note, ciliary length in this cell line remains largely unchanged upon AGRP treatment (Figure S8), suggesting both that 1) AGRP drives ciliary MC4R import and 2) that in the absence of ligand, MC4R tonic activity drives its ciliary exit without ciliary shortage. Interestingly, the conservation of ciliary length was clearly observable in our cell culture system when the acetylated tubulin staining –a main axonemal component of primary cilia– was used as a proxy for this parameter (Figure S8).

These results indicate that MC4R ciliary accumulation is cell autonomous and occurs through a dynamic re-localization of the receptor, rather than through changes in the ciliary structure.

Anatomical differences in MC4R enrichment at cilia at increasing levels of energy-deficit

Our finding that AGRP directly increases MC4R accumulation at primary cilia at longer time scales is consistent with AGRP signaling being volumetric rather than synaptic. AGRP is produced almost exclusively by ARC^{AGRP} neurons of the hypothalamus. We therefore hypothesized that MC4R cilia enrichment at anatomical regions at a greater distance from the Arcuate nucleus would differentially be affected by energy deficit. We focused specifically on the Lateral Olfactory tract (LOT) a region known to contain a large proportion of MC4R expressing neurons and that can be imaged on the same sections than the PVN (Figure 7a). As a positive control, we determined the cilia enrichment of MC4R-GFP in the LOT after ICV AGRP infusion (Figure 7b-f). Similarly to the PVN, we find that MC4R-GFP was detected at cilia in 65% of LOT neurons, and that levels of MC4R were significantly increased. This result indicates that AGRP affects MC4R dynamic similarly in the PVN and in the LOT.

We then examined whether calorie restriction impacts MC4R-GFP localization at cilia in the LOT as compared to the PVN. Unlike in the PVN, there was no change in the proportion of MC4R-GFP positive LOT neuronal cilia (Figure 7b-f) after a 24h fast. However, 10 days of 30% calorie restriction increased the proportion of MC4R-GFP positive LOT neuronal cilia. These results suggest that volumetric signaling by AGRP allows for anatomical differences in MC4R enrichment at cilia at increasing levels of energy-deficit.

Discussion

Understanding how neurons transmit and store information has focused on synaptic signaling where information may be encoded through the rate and timing of action potentials as well as through synaptic plasticity. However, neurons also transmit signals via volumetric signaling, which involves the diffusion and spread of signaling molecules like neuromodulators and growth factors through the extracellular space, thereby allowing for widespread anatomical influences

over longer timescales [120,114,121]. Here, we show that target neurons can encode volumetric signals over these long timescales by altering the composition of their primary cilia.

Specifically, we investigated how increasing energy deficits, communicated to the brain by decreased leptin levels, led to proportional accumulation of inactive MC4R at primary cilia through volumetric signaling by the MC4R inverse agonist AGRP. In our model, the progressive compensation of energy deficits, and concomitant normalization of leptin levels, would lead to decrease in AGRP and progressive exit of MC4R from cilia until low amount of activable receptor remain, and food intake is suppressed.

While most AGRP-producing neurons reside in the ARC, they project broadly throughout the brain and AGRP is released extra-synaptically along these projections[32]. MC4R ciliary accumulation occurred only with longer calorie restriction in the LOT as compared to the PVN, where it occurred after just 12 hours of fasting. Therefore, we propose that, with increased levels and duration of calorie restriction, AGRP progressively accumulates in the extracellular space in anatomical regions further away from ARC neuronal projections. Expanding domains of MC4R accumulation at neuronal cilia is a molecular and cellular basis for understanding how increased levels of energy deficit can engage increasing number of brain regions and behaviors in promoting the return to homeostasis.

In conclusion we describe a novel molecular and cellular mechanism for the brain to encode information related to energy deficit over long time scales. This finding is also highly relevant for the treatment of obesity by providing a possible cellular and molecular basis for the failure to maintain weight loss after dietary or pharmacological interventions.

Figures

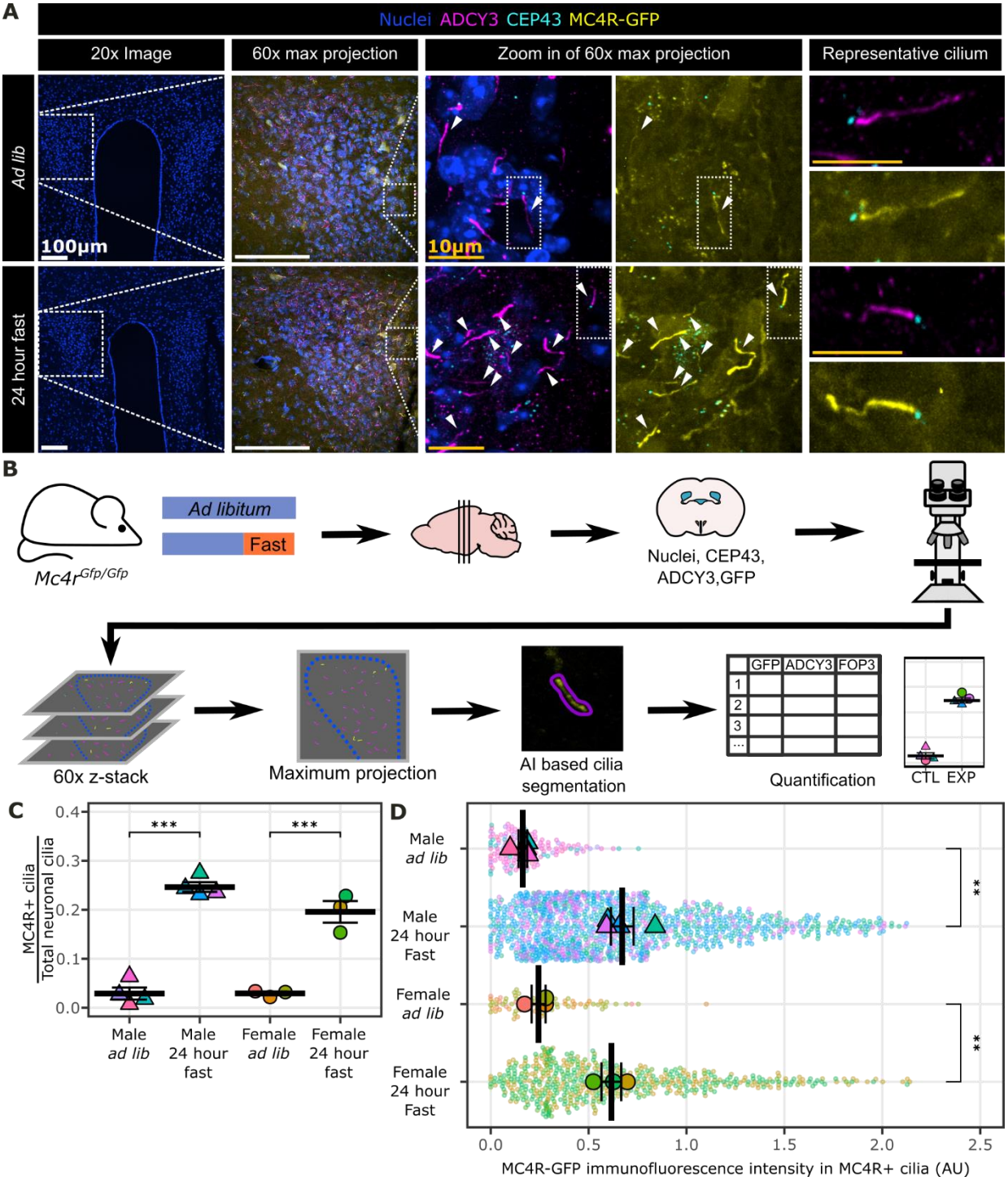


Figure 2.1 Fasting increases MC4R localization to primary cilia.

(A) Immunofluorescence images of the PVN of *ad libitum*-fed (*ad lib*, upper row) and 24hour-fasted mice (24hour fast, lower row). Increasing magnification in panels from left to right: white

dashed line boxes indicate regions magnified in the following panels. Nuclei (blue), ADCY3 (magenta), CEP43 (cyan), and MC4R-GFP (yellow). Arrowheads indicate cilia at which MC4R-GFP localizes. Scale bars: white, 100µm; orange, 10µm.

(B) Schematic of cilia analysis. *Mc4r*$^{Gfp/Gfp}$ brain cryosections are stained for nuclei, a basal body marker (CEP43), neuronal cilia marker (ADCY3), and MC4R-GFP (GFP). Z-stacks are collected with a confocal microscope at 60x magnification of 3 regions of the PVN: middle (Bregma= -0.82mm), anterior (Bregma=-0.70mm) and posterior (Bregma=-0.94mm). Cilia are automatically segmented on 60x maximum projections and data are exported for quantitative analysis. This process is described in detail in the methods.

(C) Proportion of neuronal PVN cilia to which MC4R-GFP localizes in *ad lib*-fed mice and 24hr-fasted mice. χ^2 tests are conducted between *ad lib* fed and 24hr fasted males (n=4 mice/group); and between *ad lib* fed and 24hr fasted females (n=3 mice/ group); p<0.001 for each test.

(D) Superplot of MC4R-GFP immunofluorescence intensities in MC4R-GFP positive PVN cilia detected in *ad lib*-fed and 24hr-fasted mice. Individual cilia intensities are represented as small dots (total n=1860 cilia detected across 80images). Average intensity per mouse is represented by the larger symbols (disks or triangles) and each mouse is represented with a specific colour. Welch t-test were performed on mouse averages, p=0.001 between male groups, p=0.005 between female groups. Welch t-test performed on individual cilia: p<0.001 between male groups and between female groups.

Statistics: Mouse averages are represented by black lines ± s.e.m. p-value: **<0.01, ***<0.001

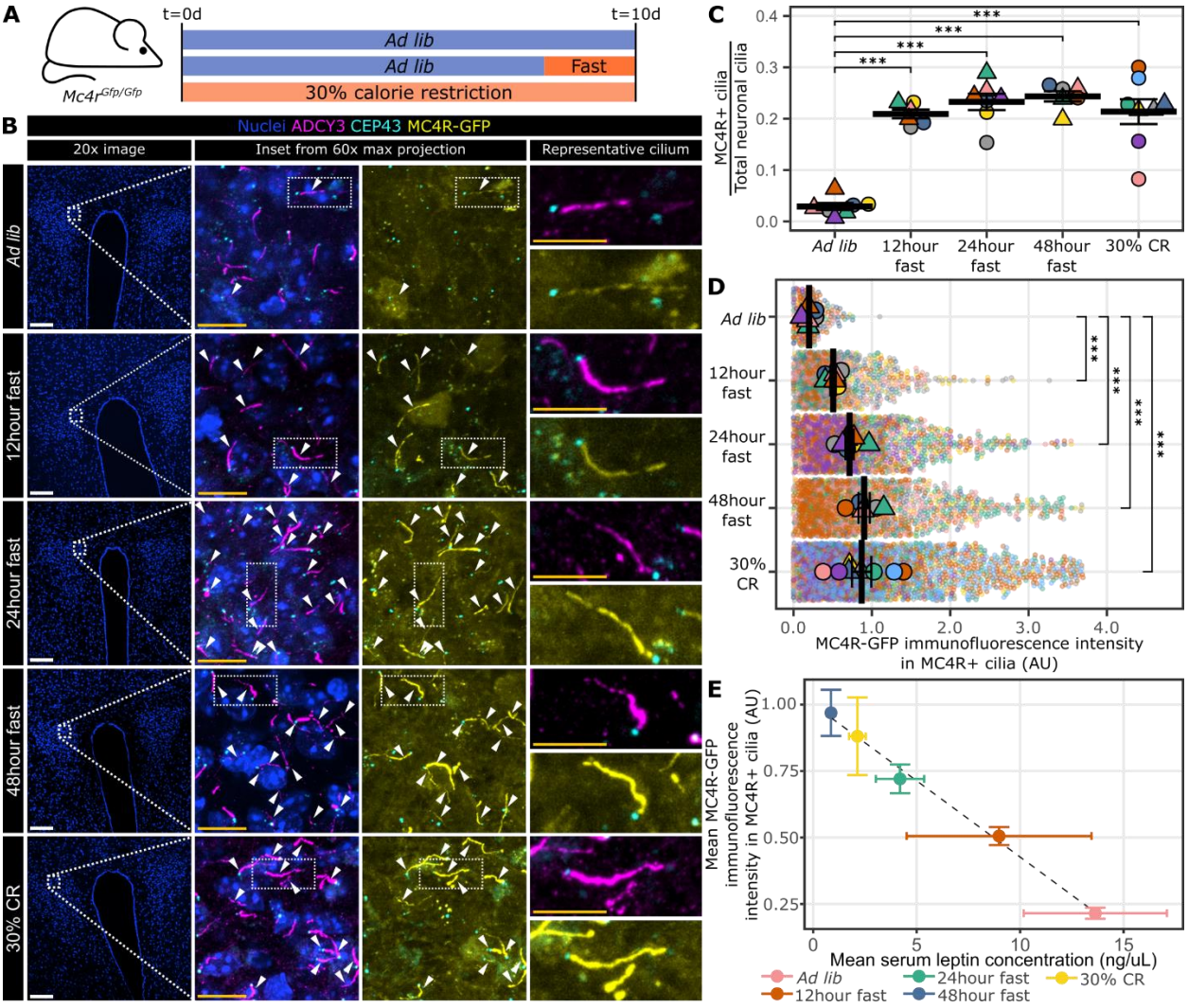


Figure 2.2: MC4R enrichment at primary cilia mirrors energy deficit

(A) Experimental design. Mice were *ad lib* fed, fasted or calorie restricted.

(B) Immunofluorescence images of the PVN from mice that were, from top to bottom, *ad lib*-fed (n=7), 12hour-fasted (n=6), 24hour-fasted (n=7), 48hour fasted (n=6), and 30% calorie-restricted (n=8). PVN image on the left. White square/rectangle indicates region magnified in subsequent panels. 60x max projection insets: CEP43 (cyan) with nuclei (blue) and ADCY3 (magenta), or MC4R-GFP (yellow). Representative cilium: CEP43 with ADCY3 or MC4R-GFP. Arrowheads indicate cilia at which MC4R-GFP localizes. Scale bars: white, 100µm; orange, 10µm.

(C) Proportion of MC4R-GFP-positive cilia among neuronal cilia in the PVN in each dietary condition, each datapoint representing the value for an individual mouse. χ^2 test conducted globally ($p<0.001$) and pairwise ($p<0.001$ *ad lib* and all other conditions).

(D) MC4R-GFP ciliary immunofluorescence intensities in MC4R-GFP positive cilia in the PVN across dietary conditions. Each dot reports the MC4R-GFP immunofluorescence intensity of a cilium (n=7252 cilia across 197 images). Symbols indicate the average per mouse (disks, females; n=3-5 per group; triangles, males; n= 3-4 per group). Welch *t*-test on averages, $p<0.001$ between *ad lib* and all other conditions. Statistics: Mouse averages are represented by black lines ± s.e.m. p-value: *<0.05, **<0.01, ***<0.001.

(E) Graph of mean serum leptin levels versus fluorescence mean intensity in PVN MC4R-GFP-positive cilia. Dots indicate average values. Error bars represent ± s.e.m. Pearson's correlation coefficient, 0.99, $p<0.001$

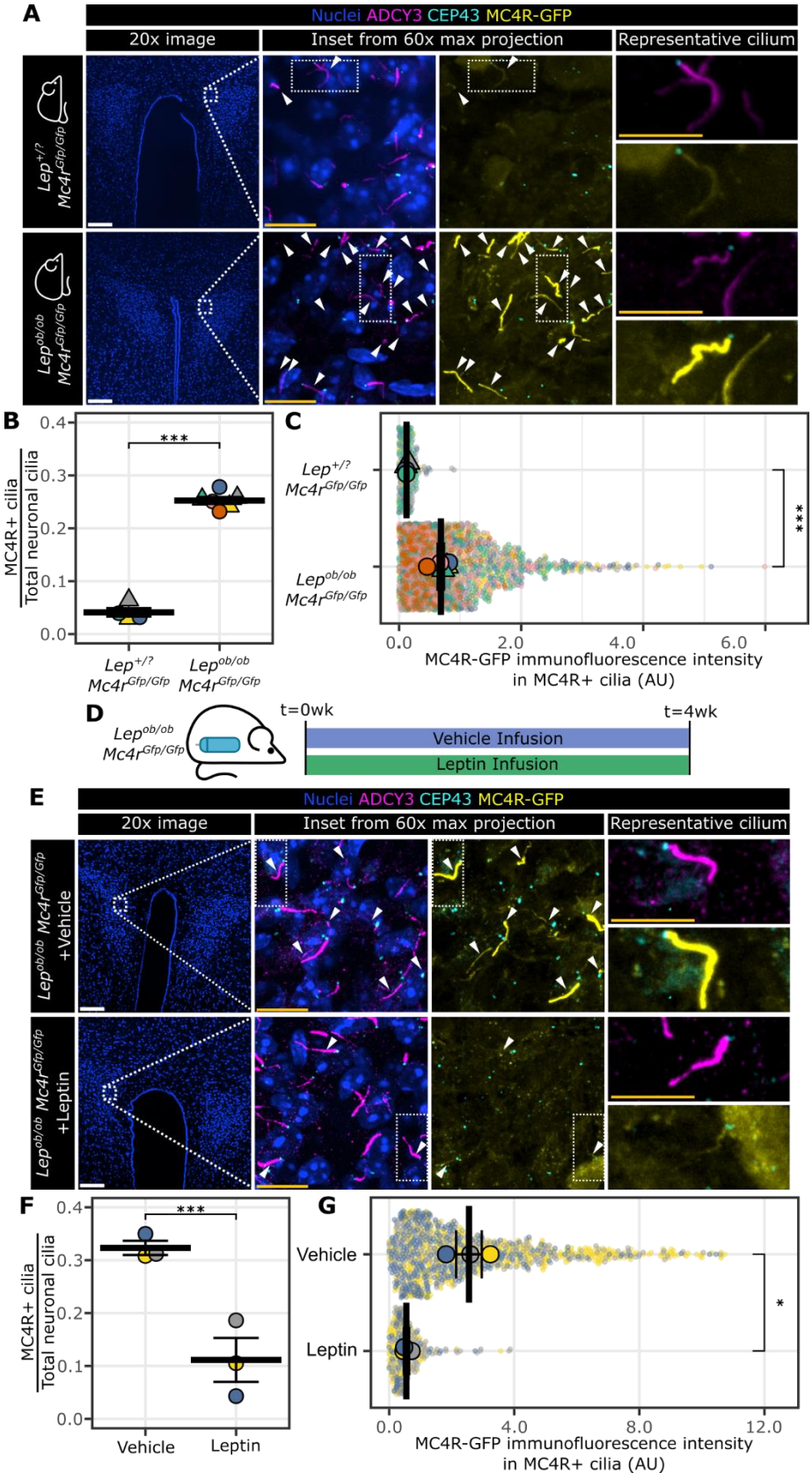

A
Nuclei ADCY3 CEP43 MC4R-GFP
20x image
Inset from 60x max projection
Representative cilium
Lep+/? Mc4rGfp/Gfp
Lepob/ob Mc4rGfp/Gfp
B
MC4R+ cilia / Total neuronal cilia
***
Lep+/? Mc4rGfp/Gfp
Lepob/ob Mc4rGfp/Gfp
C
Lep+/? Mc4rGfp/Gfp
Lepob/ob Mc4rGfp/Gfp
***
MC4R-GFP immunofluorescence intensity in MC4R+ cilia (AU)
D
Lepob/ob Mc4rGfp/Gfp
t=0wk
t=4wk
Vehicle Infusion
Leptin Infusion
E
Nuclei ADCY3 CEP43 MC4R-GFP
20x image
Inset from 60x max projection
Representative cilium
Lepob/ob Mc4rGfp/Gfp +Vehicle
Lepob/ob Mc4rGfp/Gfp +Leptin
F
MC4R+ cilia / Total neuronal cilia
***
Vehicle
Leptin
G
Vehicle
Leptin
*
MC4R-GFP immunofluorescence intensity in MC4R+ cilia (AU)

Figure 2.3: Leptin decreases ciliary MC4R level

(A) Immunofluorescence images of the PVN of 7–9-week-old *Lep*$^{+/?}$ *Mc4r*$^{Gfp/Gfp}$ (n=4) and *Lep*$^{ob/ob}$ *Mc4r*$^{Gfp/Gfp}$ littermates (n=6). PVN image on the left. White square/rectangle indicates region magnified in subsequent panels. 60x max projection insets: CEP43 (cyan) with nuclei (blue) and ADCY3 (magenta), or MC4R-GFP (yellow). Representative cilium: CEP43 with ADCY3 or MC4R-GFP. Arrowheads indicate cilia with MC4R-GFP. Scale bars: white, 100µm; orange, 10µm.

(B) Proportion of MC4R-GFP-positive cilia among neuronal cilia in the PVN of *Lep*$^{+/?}$ *Mc4r*$^{Gfp/Gfp}$ and *Lep*$^{ob/ob}$ *Mc4r*$^{Gfp/Gfp}$ mice. Each datapoint represents the value for one mouse. χ^2 tests, p<0.001.

(C) Levels of MC4R-GFP in MC4R-positive cilia from the PVN of *Lep*$^{+/?}$ *Mc4r*$^{Gfp/Gfp}$ and *Lep*$^{ob/ob}$ *Mc4r*$^{Gfp/Gfp}$ littermates. Each dot reports the MC4R-GFP immunofluorescence intensity of a cilium (n=2,618); symbols are averages per mouse (disk=females [n=2-3/group]; triangle=male [n=2-3/group]) Welch *t*-test on averages, p<0.001.

(D) Experimental design. 6-week-old *Lep*$^{ob/ob}$ *Mc4r*$^{Gfp/Gfp}$ females were infused with leptin or vehicle for 4 weeks (n=3 per group).

(E) Immunofluorescence images of the PVN of *Lep*$^{ob/ob}$ *Mc4r*$^{Gfp/Gfp}$ mice infused with vehicle or leptin. Same panel format as (A).

(F) Proportion of MC4R-positive cilia among neuronal cilia in indicated experimental groups. Each datapoint represents the value for one mouse. χ^2 tests, p<0.001.

(G) Levels of MC4R-GFP in MC4R-positive cilia from the PVN of indicated experimental groups. Each dot reports the MC4R-GFP immunofluorescence intensity of a cilium (n=1,369); symbols are averages per mouse (disk, females, n=3 per group). Welch *t*-test on mouse averages, p=0.035.

Statistics: Mouse averages are represented by black lines ± s.e.m. p-value: *<0.05, **<0.01, ***<0.001.

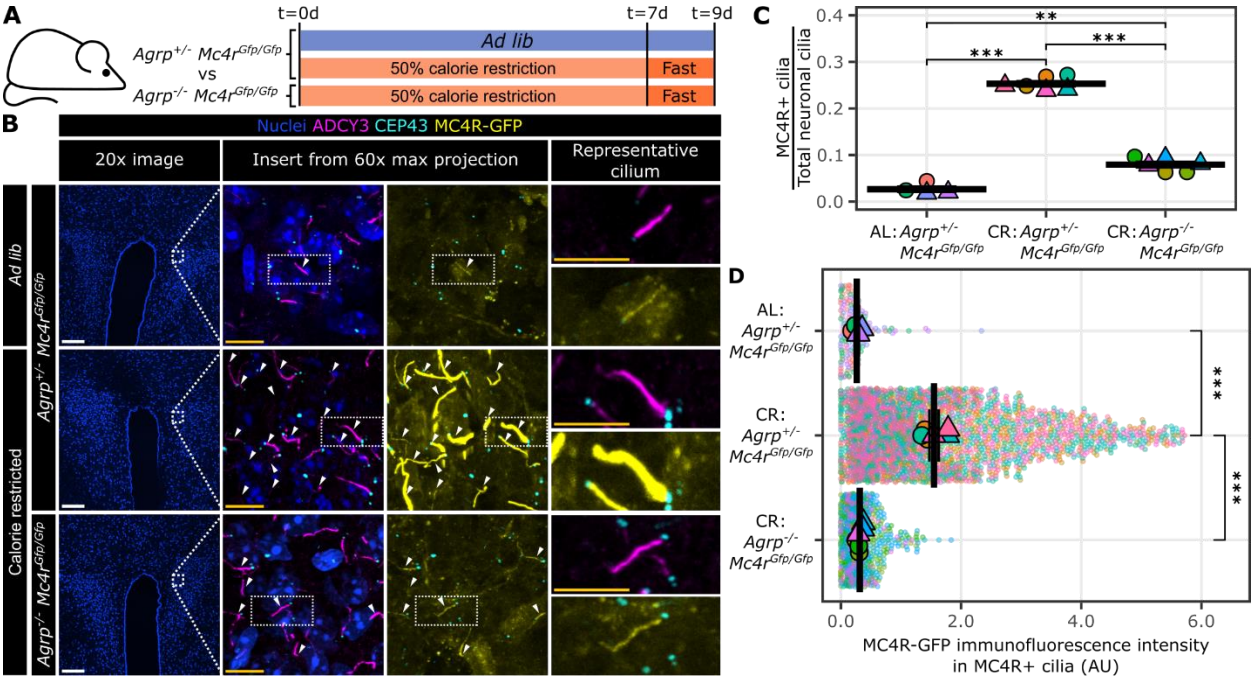


Figure 2.4: AGRP is required for MC4R accumulation at primary cilia.

(A) Experimental design. *Agrp*$^{+/-}$ *Mc4r*$^{Gfp/Gfp}$ and *Agrp*$^{-/-}$ *Mc4r*$^{Gfp/Gfp}$ mice were fed *ad lib* (n=4) or calorie restricted then fasted (n=6 per genotype).

(B) Immunofluorescence images of the PVN of *ad lib*-fed *Agrp*$^{+/-}$ *Mc4r*$^{Gfp/Gfp}$, calorie-restricted *Agrp*$^{+/-}$ *Mc4r*$^{Gfp/Gfp}$, and calorie-restricted *Agrp*$^{-/-}$ *Mc4r*$^{Gfp/Gfp}$ mice. PVN image on the left. White square/rectangle indicates region magnified in subsequent panels. 60x max projection insets: CEP43 (cyan) with nuclei (blue) and ADCY3 (magenta), or MC4R-GFP (yellow). Representative cilium: CEP43 with ADCY3 or MC4R-GFP. Arrowheads indicate cilia to which MC4R-GFP localizes. Scale bars: white, 100µm; orange, 10µm.

(C) Proportion of MC4R-GFP-positive cilia among neuronal cilia in the PVN across experimental groups, each datapoint represents the value for one mouse. χ^2 test, p=0.010 between *ad lib* *Agrp*$^{+/-}$ *Mc4r*$^{Gfp/Gfp}$ and calorie restricted *Agrp*$^{-/-}$ *Mc4r*$^{Gfp/Gfp}$, p<0.001 for the rest of the comparisons.

(D) Levels of MC4R-GFP in MC4R-positive cilia in the PVN of indicated experimental groups. Each dot reports the MC4R-GFP immunofluorescence intensity of a cilium (n= 3,342); each symbol, the average per mouse (disks, females, n=2-3 per group; triangles, males n=2-3 per group). Welch *t*-tests on mouse averages, p<0.001 for all comparisons except between *ad lib*-fed *Agrp*$^{+/-}$ *Mc4r*$^{Gfp/Gfp}$ and calorie-restricted *Agrp*$^{-/-}$ *Mc4r*$^{Gfp/Gfp}$ where p=0.302.

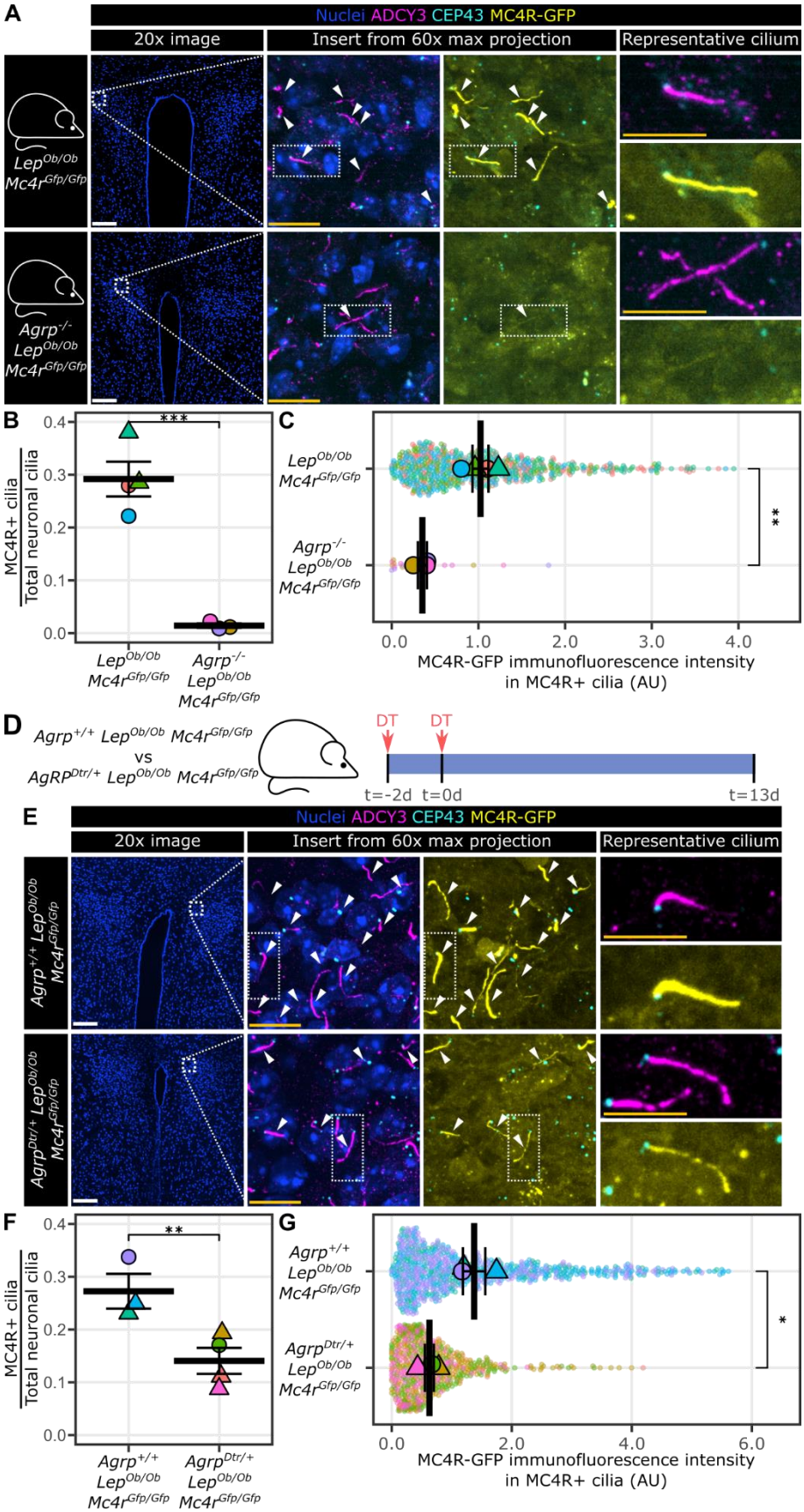

A
Nuclei ADCY3 CEP43 MC4R-GFP
20x image
Insert from 60x max projection
Representative cilium
Lep^Ob/Ob Mc4r^Gfp/Gfp
Agrp^-/- Lep^Ob/Ob Mc4r^Gfp/Gfp
B
MC4R+ cilia / Total neuronal cilia
***
C
MC4R-GFP immunofluorescence intensity in MC4R+ cilia (AU)
**
D
Agrp^+/+ Lep^Ob/Ob Mc4r^Gfp/Gfp
vs
AgRP^Dtr/+ Lep^Ob/Ob Mc4r^Gfp/Gfp
DT
DT
t=-2d t=0d
t=13d
E
Nuclei ADCY3 CEP43 MC4R-GFP
20x image
Insert from 60x max projection
Representative cilium
Agrp^+/+ Lep^Ob/Ob Mc4r^Gfp/Gfp
Agrp^Dtr/+ Lep^Ob/Ob Mc4r^Gfp/Gfp
F
MC4R+ cilia / Total neuronal cilia
**
G
MC4R-GFP immunofluorescence intensity in MC4R+ cilia (AU)
*

Figure 2.5: AGRP is required to promote MC4R accumulation in primary cilia of leptin-deficient mice.

(A) Immunofluorescence images of the PVN of *Agrp* control (*Lep*$^{ob/ob}$ *Mc4r*$^{Gfp/Gfp}$, n=4, top panels) and *Agrp* mutant (*Agrp*$^{-/-}$ *Lep*$^{ob/ob}$ *Mc4r*$^{Gfp/Gfp}$, n=3, bottom panels) mice. From left to right: PVN image with white square indicating region magnified in the next 2 panels, insert from 60x maximum projection; magnified region of 60x showing representative cilia. Nuclei (blue), ADCY3 (magenta), and CEP43 (cyan); or MC4R-GFP (yellow) and CEP43 (cyan). Arrowheads indicate cilia positive for MC4R-GFP. Scale bars: white, 100µm; orange, 10µm.

(B) Proportion of MC4R-positive cilia among neuronal cilia in the PVN in each group, each datapoint representing the value for an individual mouse. $\chi 2$ test, $p<0.001$.

(C) Level of MC4R accumulation, in MC4R-positive cilia of the PVN, in indicated groups. Each dot represents an individual cilium MC4R-GFP immunofluorescence intensity (total n=671); each symbol, the average per mouse (disks, females, n=2-3/group; triangles, males n=0-2/group). Welch t-test on mouse averages, p=0.002.

(D) Experimental design for parts E-G. AGRP neuron conditional loss (*Agrp*$^{Dtr/+}$ *Lep*$^{ob/ob}$ *Mc4r*$^{Gfp/Gfp}$, n=3) and control (*Agrp*$^{+/+}$ *Lep*$^{ob/ob}$ *Mc4r*$^{Gfp/Gfp}$, n=4) mice received two doses of diphtheria toxin (DT) and were perfused 13 days later.

(E) Immunofluorescence images of the PVN from *Agrp*$^{+/+}$ *Lep*$^{ob/ob}$ *Mc4r*$^{Gfp/Gfp}$ (top) and *Agrp*$^{Dtr/+}$ *Lep*$^{ob/ob}$ *Mc4r*$^{Gfp/Gfp}$ mice (bottom). From left to right: same panel format as A.

(F) Proportion of PVN cilia to which MC4R-GFP localizes in indicated groups, each datapoint representing the value for an individual mouse. $\chi 2$ test, $p=0.004$.

(G) Level of MC4R accumulation, in MC4R-positive cilia of the PVN, in indicated groups. Each dot represents an individual cilium MC4R-GFP immunofluorescence intensity (total n=1408); each symbol, the average per mouse (disks, females, n=1/group; triangles, males n=2-3/group). Welch t-test on mouse averages, p=0.043.

Statistics: Mouse averages are represented by black lines ± s.e.m. p-value: *<0.05, **<0.01, ***<0.001.

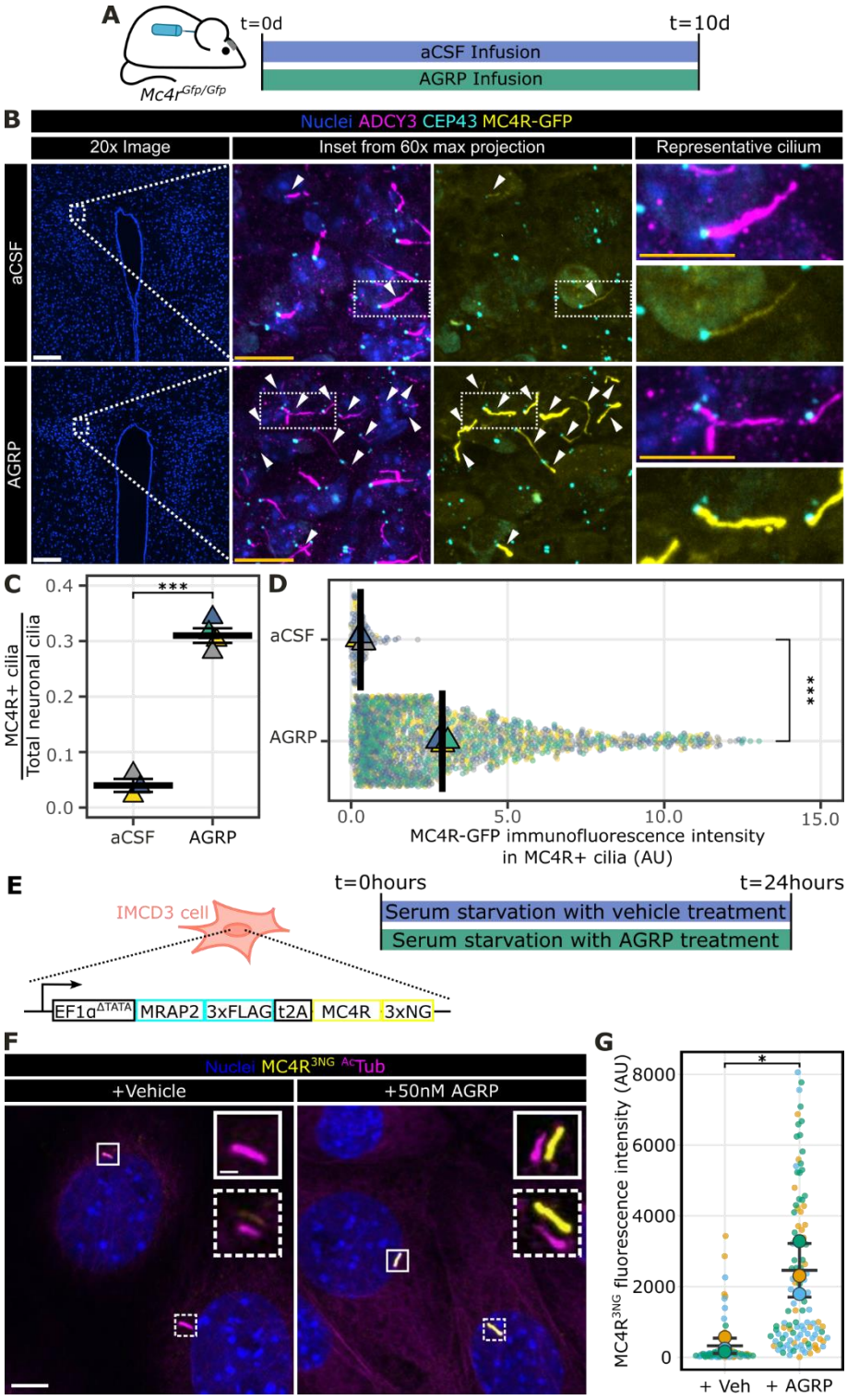


Figure 2.6: AGRP drives MC4R accumulation at primary cilia in vivo and cell-autonomously

(A) Experimental design. *Mc4r*$^{Gfp/Gfp}$ mice were infused intracerebroventricularly with aCSF (n=3) or AGRP (n=4) for 10 days.

(B) Immunofluorescence images of the PVN of *Mc4r*$^{Gfp/Gfp}$ mice infused with aCSF or AGRP. PVN image on the left. White square/rectangle indicates region magnified in subsequent panels. 60x max projection insets: CEP43 (cyan) with nuclei (blue) and ADCY3 (magenta), or MC4R-GFP (yellow). Representative cilium: CEP43 with ADCY3 or MC4R-GFP. Arrowheads indicate MC4R-GFP+ cilia. Scale bars: white, 100µm; orange, 10µm.

(C) Proportion of MC4R-GFP-positive cilia among neuronal cilia in the PVN, Each datapoint represents the value for one mouse. χ^2 test, p<0.001

(D) Levels of MC4R-GFP in MC4R-positive cilia in the PVN of indicated experimental groups. Each dot reports the MC4R-GFP immunofluorescence intensity of a cilium (n=1,925); symbol indicate the average intensity per mouse (triangles, males n=3-4 per group). Welch *t*-test on mouse averages, p<0.001.

Statistics: Mouse averages are represented by black lines ± s.e.m. p-value: *<0.05, **<0.01, ***<0.001.

(E) Experimental design for F and G. IMCD3 cells with stable expression of MC4R-3xNeonGreen and MRAP2 treated with vehicle or AGRP.

(F) Images of these IMCD3 cells treated with vehicle (left) or AGRP (right) were stained for cilia (TUB^{Ac}, magenta), DNA (blue) and imaged for MC4R-3xNeonGreen (yellow). Insets show offset images of representative cilia. Scale bar, 5 µm; insets, 1 µm.

(G) MC4R-3xNeonGreen ciliary fluorescence intensity in vehicle-treated and AGRP-treated cells. Each small dot represents the fluorescence intensity in one cilia and big disks the mean of one experiment (n=3 independent experiments, 35-50 cilia each). Black lines represent the mean of all experiments ± SD. Welch *t*-test on experimental replicates (*p-value=0.032).

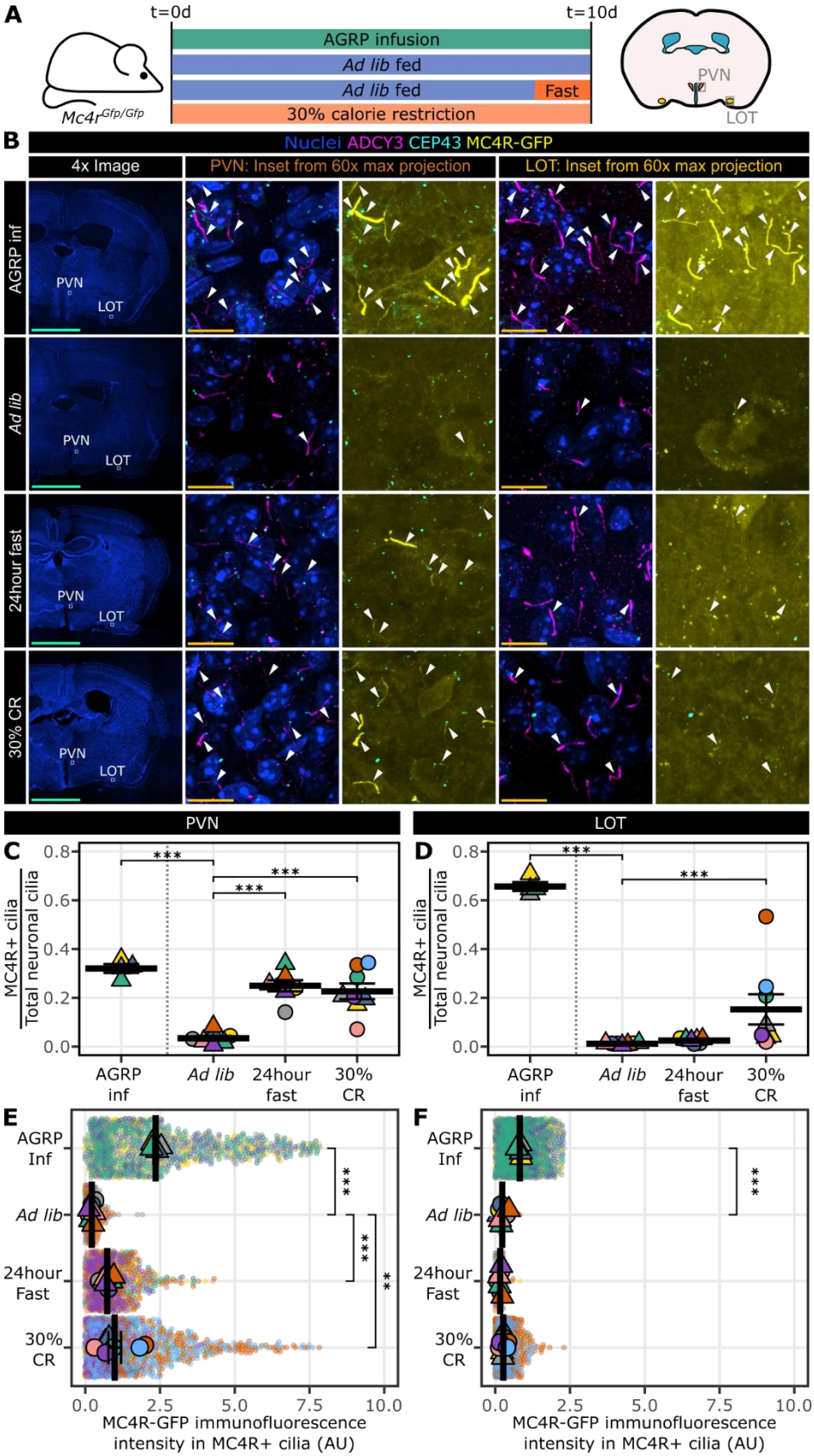

A
t=0d
t=10d
AGRP infusion
Ad lib fed
Ad lib fed
Fast
30% calorie restriction
Mc4r Gfp/Gfp
PVN
LOT
B
Nuclei ADCY3 CEP43 MC4R-GFP
4x Image
PVN: Inset from 60x max projection
LOT: Inset from 60x max projection
AGRP inf
Ad lib
24hour fast
30% CR
PVN
LOT
PVN
LOT
C
D
MC4R+ cilia / Total neuronal cilia
0.0
0.2
0.4
0.6
0.8
***
AGRP inf
Ad lib
24hour fast
30% CR
E
F
AGRP Inf
Ad lib
24hour Fast
30% CR
**
0.0
2.5
5.0
7.5
10.0
MC4R-GFP immunofluorescence intensity in MC4R+ cilia (AU)

Figure 2.7: Anatomical differences in MC4R ciliary enrichment with increasing levels of energy-deficit

(A) Experimental Design. *Mc4r*$^{Gfp/Gfp}$ mice were *ad lib* fed, fasted, calorie-restricted, or infused with AGRP.

(B) Immunofluorescence images of the PVN and LOT of *Mc4r*$^{Gfp/Gfp}$ mice that were AGRP infused (n=4), *ad lib* fed (n=7), fasted for 24hrs (n=7), or calorie restricted (n=8). Images of the PVN and LOT were taken from the same section. Left panel: brain section; white square indicates region magnified in insets of the PVN (left) and LOT (right). Insets show CEP 43 (cyan) with nuclei (blue) and ADCY3 (magenta), or MC4R-GFP (yellow). Arrowheads indicate MC4R-GFP-positive cilia. Scale bars: teal, 2000µm; orange, 10µm.

(C-D) Proportion of MC4R-GFP-positive cilia among PVN (C) and LOT (D) neuronal cilia in indicated experimental groups. Each datapoint represents the value for one mouse. χ^2 test, $p<0.001$ except in the LOT between *ad lib* fed and 24hr fast, $p=0.936$.

(E-F) Levels of MC4R-GFP in MC4R-positive cilia in the PVN (E) or LOT (F) of indicated experimental groups. Each dot reports the MC4R-GFP immunofluorescence intensity of a cilium (PVN: n= 4,072; LOT: n=2,965); symbols indicate averages per mouse (disks, females, n=0-5 per group; triangles, males n=3-4 per group). Welch *t*-test performed on mouse averages: $p<0.001$, PVN: between *ad lib* and AGRP infused or 24hour fasted, LOT: between *ad lib* and AGRP infused; $p=0.008$, PVN: between ad lib and calorie restricted; non-significant, LOT: between *ad lib* and 24hour-fasted ($p=0.245$) or calorie restricted mice ($p=0.595$).

Statistics: Mouse averages are represented by black lines ± s.e.m. p-value: *<0.05, **<0.01, ***<0.001.

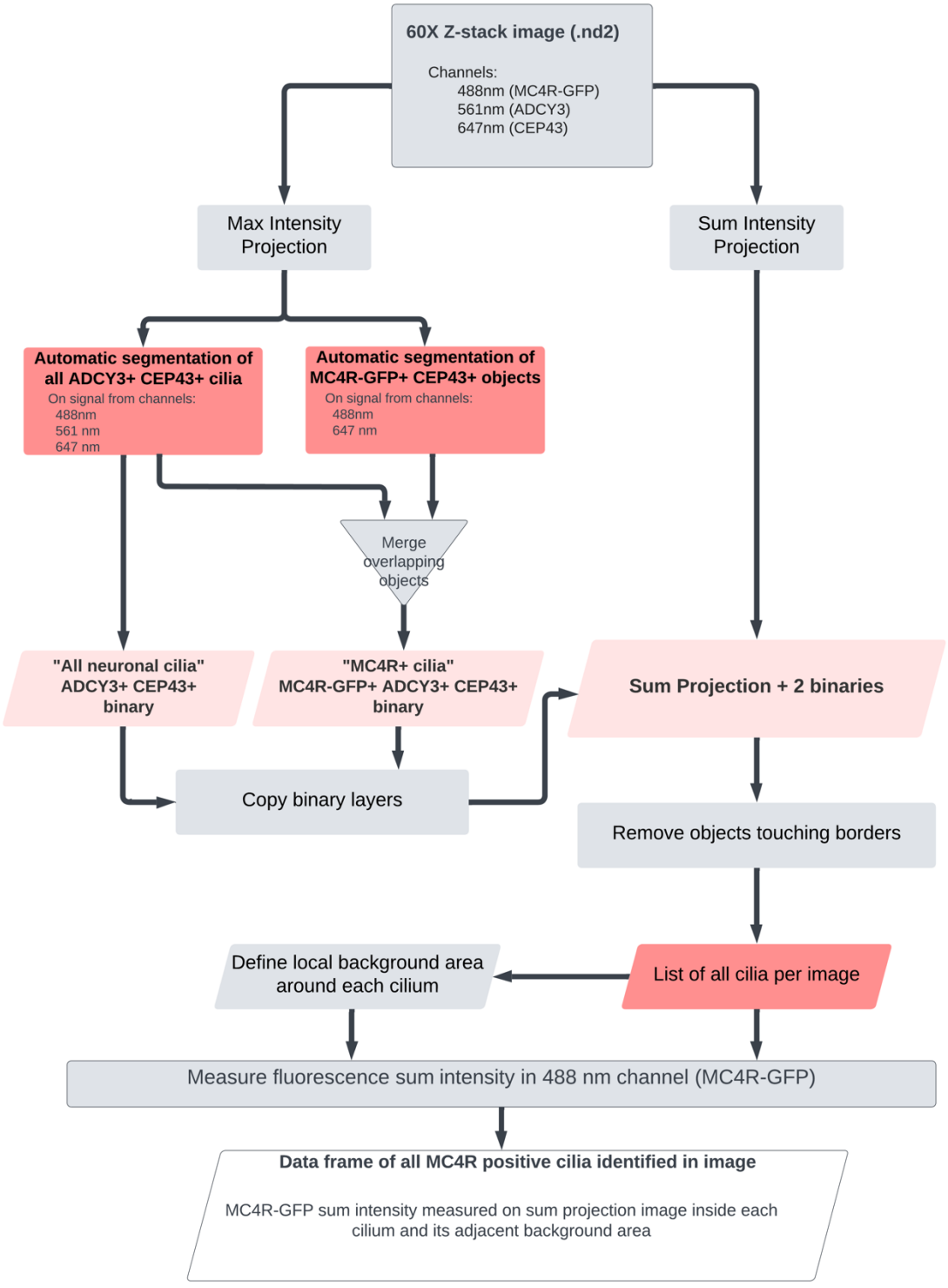

60X Z-stack image (.nd2)
Channels:
488nm (MC4R-GFP)
561nm (ADCY3)
647nm (CEP43)
Max Intensity Projection
Sum Intensity Projection
Automatic segmentation of all ADCY3+ CEP43+ cilia
On signal from channels:
488nm
561 nm
647 nm
Automatic segmentation of MC4R-GFP+ CEP43+ objects
On signal from channels:
488nm
647 nm
Merge overlapping objects
"All neuronal cilia" ADCY3+ CEP43+ binary
"MC4R+ cilia" MC4R-GFP+ ADCY3+ CEP43+ binary
Sum Projection + 2 binaries
Copy binary layers
Remove objects touching borders
Define local background area around each cilium
List of all cilia per image
Measure fluorescence sum intensity in 488 nm channel (MC4R-GFP)
Data frame of all MC4R positive cilia identified in image
MC4R-GFP sum intensity measured on sum projection image inside each cilium and its adjacent background area

Figure 2.8- Supplemental Figure S1: Quantification of ciliary MC4R localization using AI segmentation models.

To quantify the localization of MC4R at the primary cilium, we used the Nis.ai module of the NIS-Element software (Nikon) to develop an automated segmentation approach. We trained two NIS.ai models to segment all neuronal primary cilia (ADCY3+ CEP43+) and MC4R-GFP positive cilia (MC4R-GFP+ ADCY3+ CEP43+) on a maximum intensity projection of each raw z-stack image (see supplementary methods). The binaries were then transferred to a sum projection of the 60x z-stack image for quantification of MC4R-GFP fluorescence inside each individual primary cilium. Local background fluorescence was subtracted individually for each cilium and objects with lengths below 3µm or touching image borders were excluded from the final list of cilia for downstream analysis.

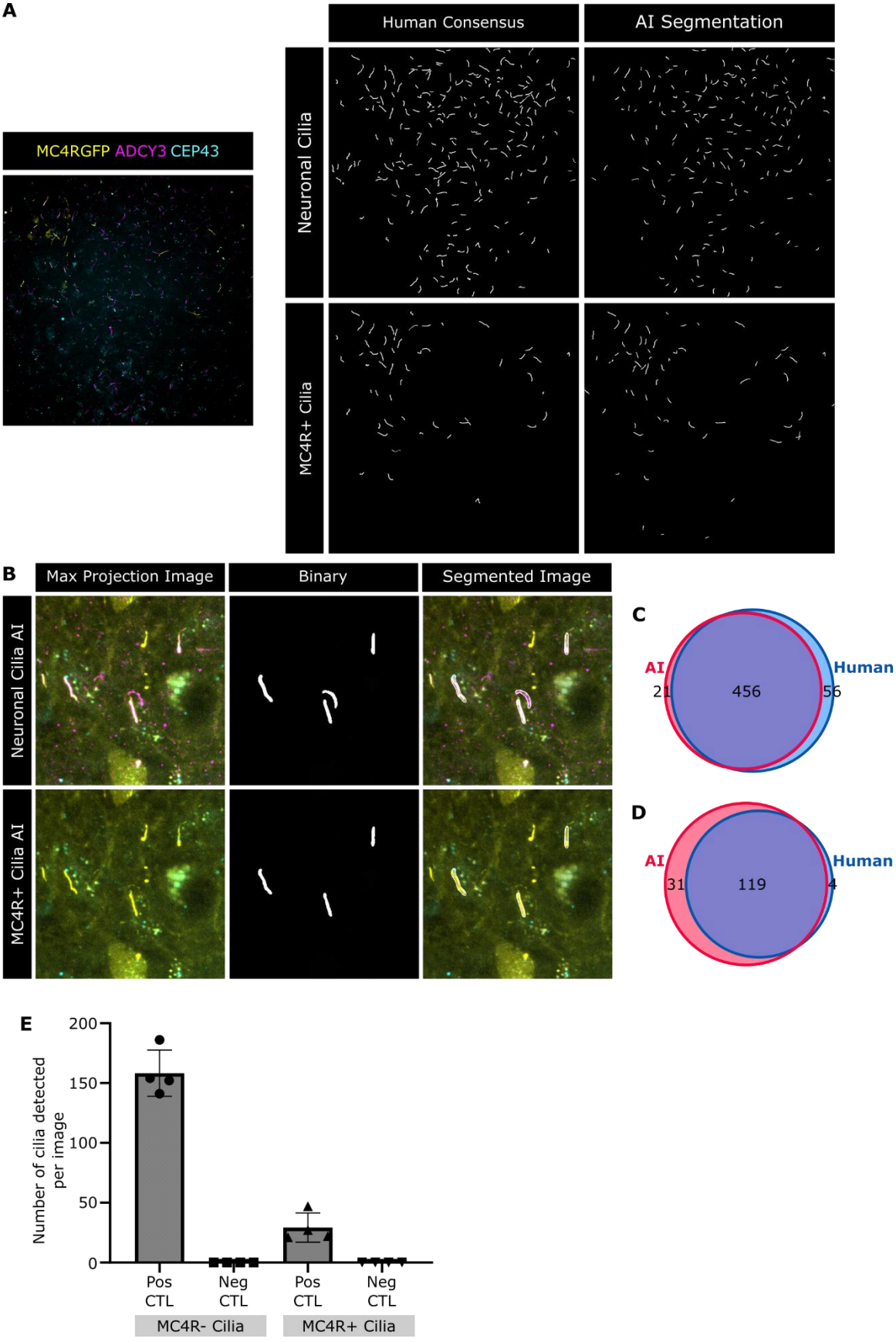

A
Human Consensus
AI Segmentation
MC4RGFP ADCY3 CEP43
Neuronal Cilia
MC4R+ Cilia
B
Max Projection Image
Binary
Segmented Image
Neuronal Cilia AI
MC4R+ Cilia AI
C
AI
Human
21
456
56
D
AI
Human
31
119
4
E
Number of cilia detected per image
200
150
100
50
0
Pos CTL
Neg CTL
Pos CTL
Neg CTL
MC4R- Cilia
MC4R+ Cilia

Figure 2.9- Supplemental Figure S2: Validation of automated cilia segmentation process.

(A) 60x max projection showing MC4R-GFP (yellow), ADCY3(magenta), and CEP43 (cyan) on the far left. The columns of the 4x4 image layout show cilia segmentation by human and automatic segmentation (left to right) of all neuronal cilia (top row) and MC4R+ neuronal cilia (bottom row) in a whole wide field 60x maximum projection image.

(B) Representative region of segmented 60x maximum projections. The top row shows segmentation of all neuronal cilia based on ADCY3, CEP43, and MC4R-GFP signal. The bottom row shows segmentation of MC4R-GFP positive cilia based on CEP43 and MC4R-GFP.

(C) Accuracy of the neuronal cilia NIS.AI segmentation model represented as a Venn diagram showing the number of cilia picked up by humans only, both human and NIS.AI, and NIS.AI only.

(D) Accuracy of the MC4R-GFP positive cilia NIS.AI segmentation model represented as a Venn diagram showing the number of cilia picked up by humans only, both human and NIS.AI, and NIS.AI only.

(E) Specificity of our automated segmentation protocol. Number of MC4R negative and MC4R positive cilia picked up in the positive control image (from brain sections stained for ADCY3, CEP43 and MC4R-GFP) and negative control image (from sections not stained for ADCY3, CEP43, and MC4R-GFP).

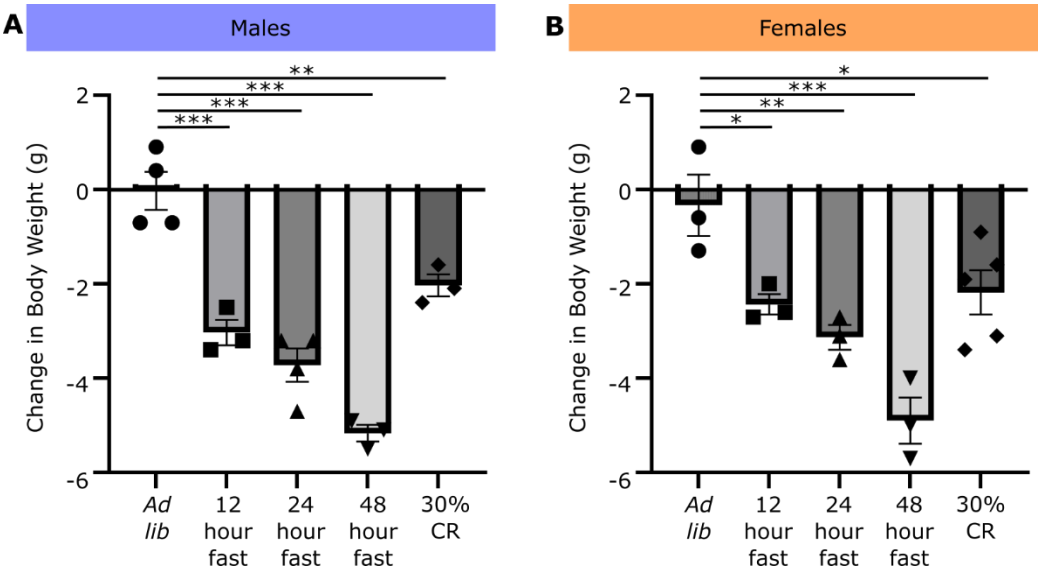


Figure 2.10- Supplemental Figure S3: Body weight change upon energy deficit.

Changes in mouse body weight after fasting and calorie restriction in males (A, n=3-4 mice per group) and females (B, n=3-5 mice per group). Male p-values: $p<0.001$ between ad lib fed and 12hr fasted, ad lib fed and 24hr fasted, and ad lib fed and 48hr fasted mice; and $p=0.003$ between ad lib fed and calorie restricted mice. Female p-values: $p=0.038$ between ad lib fed and 12hr fasted mice, $p=0.007$ between ad lib fed and 24hr fasted mice, $p<0.001$ between ad lib fed and 48hr fast mice, and $p=0.041$ between ad lib fed and calorie restricted mice.

Statistics: One way ANOVA with multiple comparisons was conducted. Error bars represent s.e.m. p-value: *<0.05 **<0.01 ***<0.001.

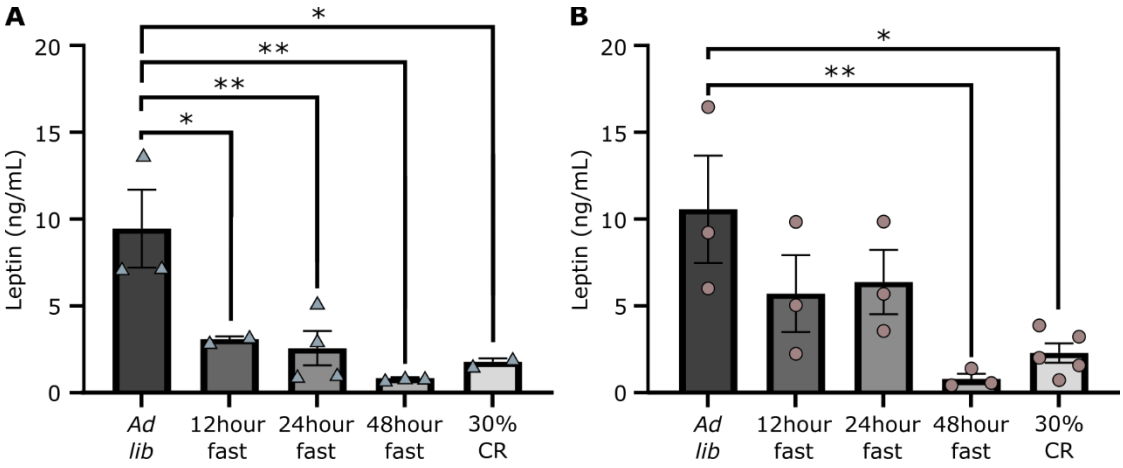


Figure 2.11- Supplemental Figure S4: Circulating leptin levels upon energy deficit.

Leptin levels in males (A, n=2-4 mice per group) and females (B, n=3-5 mice per group). Ordinary one-way ANOVA with multiple comparisons analysis was conducted to compare ad lib to all other groups. P values for males: *ad lib* vs 12hr fast p=0.033, *ad lib* vs 24hr fast p=0.008, *ad lib* vs 48hr fast p=0.003, and *ad lib* vs 30% calorie restriction p=0.012. P values for females: *ad lib* vs 48hr fast p=0.007, and *ad lib* vs 30% calorie restriction p=0.010.

Error bars represent SEM p-value: *<0.05 **<0.01 ***<0.001.

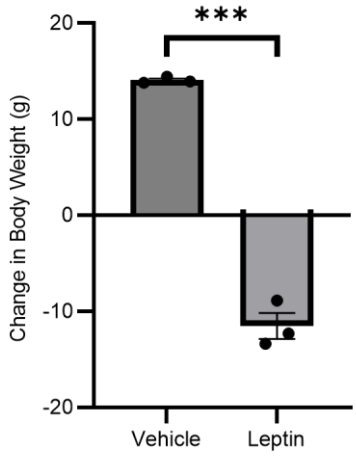


Figure 2.12- Supplememental Figure S5: Body weight change of Lep$^{ob/ob}$ Mc4r$^{Gfp/Gfp}$ mice infused with vehicle or leptin.

Change in body weight of *Lep$^{ob/ob}$ Mc4r$^{Gfp/Gfp}$* mice after 4 weeks of vehicle (n=3) or leptin (n=3) infusion. Unpaired t-test,***p<0.001. Error bars represent s.e.m.

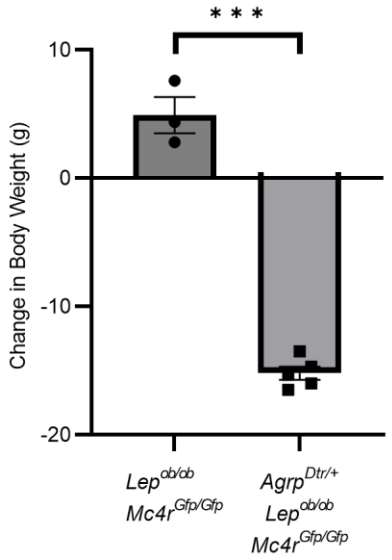


Figure 2.13- Supplemental Figure S6: Body weight change of mice with conditional loss of AGRP neurons.

Change in body weight in *Lep*$^{ob/ob}$ *Mc4r*$^{Gfp/Gfp}$ (n=3) and *Agrp*$^{Dtr/+}$ *Lep*$^{ob/ob}$ *Mc4r*$^{Gfp/Gfp}$ (n=5) mice injected with diphtheria toxin. Unpaired t-test,***p<0.001. Error bars represent s.e.m.

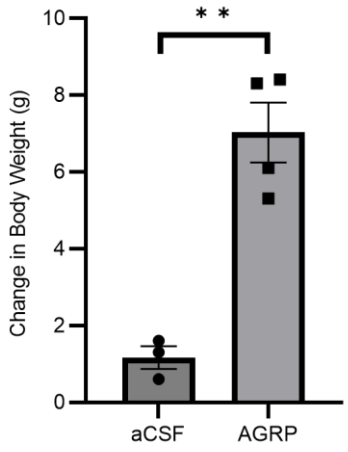


Figure 2.14- Supplemental Figure S7: Body weight change of aCSF- and AGRP- infused mice.

Change in body weight in *Mc4r*$^{Gfp/Gfp}$ mice infused with aCSF (n=3) or AGRP peptide (n=4). Unpaired t-test,(p=0.002). Error bars represent s.e.m.

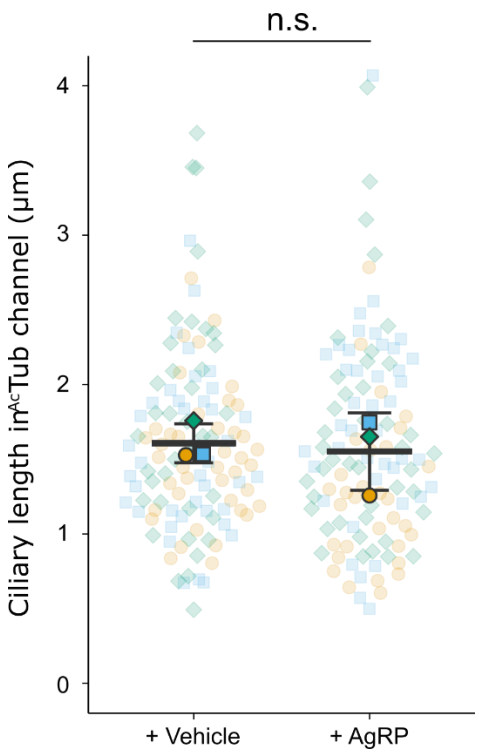


Figure 2.15- Supplemental Figure S8: AGRP does not change cilia length.

Superplot comparing cilia length of cells treated with vehicle or 50 nM AgRP. Cilia length was measured using the acetylated tubulin channel. N = 3 independent experiments, each of which comprises 35-50 quantified cilia, encoded in translucent points of different shape and color. The mean of each experiment is plotted as a solid shape. The thick black line represents the mean of all three experiments globally. The error bars represent the standard deviation of all three experiments globally. Parametric unpaired T-test performed on individual cilia p=0.7731. Welch t-test performed on independent experiment averages p=0.765.

Methods

Animals

Mice were housed in a barrier facility maintained at 23°C ± 2°C and 50-70% humidity with a 12hr light (beginning at 7am) and 12hr dark (beginning at 7pm) cycles. Animals were weaned at 4 weeks of age and fed rodent diet 5058 (Lab Diet). Experiments were performed on age-matched C57BL6/J mice. Mice were group housed (up to 5 mice per cage), except for the following experiments: they were single housed for food intake measurement, caloric restriction, or post pump implantation surgeries.

The mouse lines used are: *Mc4r*$^{tm1(egfp)Vai}$*(33-35)*, *Lep*^{ob} (IMSR_JAX:000632), *Agrp*$^{-/-}$ *(48)* (Allison Wanting Xu, UCSF) and *Agrp*$^{tm2(DTR)Rpa}$ (IMSR_JAX:033171).

Mouse metabolism studies

For caloric restriction studies: daily food intake was measured manually on single housed mice over 4 days and averaged to obtain baseline daily food intake. 30% calorie restriction was done by giving single housed mice 70% of their baseline daily food intake at the start of the dark cycle daily. 50% calorie restriction was done by giving 50% of their baseline daily food intake at the start of the dark cycle daily.

Pharmacological agents

Mouse recombinant leptin (R&D systems, 498-OB) was reconstituted in 20mM Tris-HCL, pH 7.8, (Teknova, T1080) to the concentration of 1mg/mL and diluted to 0.83mg/mL with 0.9% saline solution(Hospira Inc) prior to use. 17mM Tris-HCL, pH 7.8 was used as the vehicle in vehicle-infused controls. AgRP (Phoenix Pharmaceuticals INC., 003-57) was reconstituted in aCSF (Tocris, 3525) to the concentration of 0.2mg/mL and used for ICV infusions.

Pump Implantations

Aseptic technique was used for all pump implantation procedures.

Subcutaneous leptin pump implantations

Mini-osmotic pumps (Alzet, model 2002, 0.5 µl per hour, 14 days) were filled with leptin (0.83µg/µL) or vehicle (17mM Tris-HCl in 0.9% saline) the day before surgeries and primed overnight at 37°C in 0.9% saline solution. *Mc4r*$^{Gfp/Gfp}$ *Lep*$^{Ob/Ob}$ mice were given preoperative analgesic, Buprenex (0.3mg/kg, Covetrus), before being anesthetized with 4% isoflurane (Dechra) in an induction chamber. Anesthesia was maintained with 2%±1% isoflurane through a nose cone. During the procedure, mice were placed on top of a heating pad kept at 30°C -37°C. The upper back of the mouse was shaved, cleaned, and injected with a local anesthetic, Lidocaine (2.5mg/kg, VetOne). A 1.5cm incision was made in the skin to subcutaneously place the osmotic pump,

opening first, down the side of the mouse. The incision was sutured closed. Mice were given post operative anti-inflammatory drug, meloxicam (5mg/kg, Pivetal), and antibiotics, enrofloxacin (20mg/kg, Baytril), right after surgery and the day after surgery. Animals were single housed and monitored post-surgery to ensure recovery. Pumps were replaced after 2 weeks of infusion.

Intracerebroventricular AgRP infusion

Micro-osmotic pumps (Alzet, model 1002, 0.25 µl per hour, 14 Days) were filled with AgRP (0.2µg/µL) or aCSF the day before surgeries and primed overnight at 37°C in 0.9% saline. *Mc4r*$^{Gfp/Gfp}$ mice were given preoperative analgesic, Buprenex (0.3mg/kg, Covetrus), before being anesthetized with 4% isoflurane (Dechra) in an induction chamber. Anesthesia was maintained with 2%±1% isoflurane. Mice were placed on a heating pad (maintained at 30-37°C) in a stereotaxic frame (KOPF Model 1900). Briefly, Lidocaine (2.5mg/kg) was injected at the incision site, then a 2.5cm incision in the scalp was made to expose the skull. The skull was adjusted so that bregma and lambda of the skull are on the same plane, and points that were 2mm directly right and left from the midpoint between bregma and lambda are on the same plane. A hole in the skull was drilled (coordinates from Bregma: AP=-0.3, ML=1; Kopf, stereotaxic drill model 1911, with Kyocera, micro drill bit #95) and a 2.5mm cannula (Alzet brain infusion kit 3) was inserted into the lateral ventricle and fixed into place using dental cement. The cannula was connected to the micro-osmotic pump, which was inserted subcutaneously on the side of the back of the mouse. The incision was sutured closed. Mice were given anti-inflammatory drug (meloxicam, 5mg/kg) and antibiotics (enrofloxacin, 20mg/kg) right after surgery and the day after surgery; and single housed post-surgery. AgRP/aCSF were infused for 10 days, and body weight was monitored.

Diphtheria toxin injections

Diphtheria toxin (5ng/µL, dissolved in 0.01M PBS [Gibco, 20012-043]) was intraperitoneally injected twice: once on the first day, and again 2 days later. Each mouse was given 1µg of diphtheria toxin in each injection.

Serum leptin measurements

Blood was collected, at the end of each experiment, via cardiac puncture after anesthesia with Avertin (250-400mg/kg, Sigma Aldrich, T48402) and allowed to clot for 30min-1hour on ice. Serum was separated by centrifugation at 2000xg for 10min at. Serum leptin levels were then measured by Mouse Leptin ELISA Kit (Crystal Chem, 90030) according to the manufacturer's instructions.

Brain Imaging

At the end of each experiment, mice were perfused transcardially, immediately after blood collection, with 0.01M PBS at pH of 7.9 (Teknova, P0179), and 4% paraformaldehyde (Electron Microscopy Sciences, 15714). Brains were extracted and post-fixed in 4% PFA overnight, and

cryoprotected in 30% sucrose, before being embedded in M1 Matrix (Epredia, 1310) and stored at -80°C. Brains were then cut into 35µm coronal sections and kept in 0.01M PBS at 4°C before staining. Mice used in the experiments presented in figures 1, 4 and 5 were perfused at 8.5 weeks old; figures 2A-C at 7-9 weeks old; figure 3D-G at 10 weeks old; figure 3 at 9.5weeks old. Mice used in experiments in supplemental figure 1 were perfused at 8.5 weeks; and in supplemental figure 7A-C at 11-13weeks old; and in supplemental figure 7D-G at 16weeks old.

For image quantification, we stained and imaged 3 sections of the paraventricular nucleus (PVN) to get a survey of the whole PVN. We chose a section in the middle of the PVN (Bregma=-0.82mm), and a section anterior (Bregma=-0.7mm) and a section posterior (Bregma=-0.94mm) of the mid-PVN section. Sections were stained for nuclei, ADCY3, CEP43, and MC4R-GFP using the staining procedure described below.

The staining procedure comprised of washing sections in 0.01M PBS, then blocking them for 1 hour in blocking buffer: 10% goat serum (Jackson Immunoresearch, 005-000-121), 5% BlokHen (Aves Labs, BH-1001), 85% antibody buffer (1.125% NaCl [MilliporeSigma, S5886], 0.75% Tris base [Thermo Fisher Scientific, BP152], 1% BSA [Thermo Fisher Scientific, BP1600], 1.8 % L-Lysine [Alfa Aesar, J62225], and 0.04% sodium azide [Millipore Sigma]; pH adjusted to 7.4), and 0.3% Triton-X (Sigma, X100-500ML). Sections were incubated in primary antibody diluted in blocking buffer on an orbital shaker at 4°C overnight (chicken anti-ADCY3, antibodies.com, A104341, 1:500; rabbit anti-CEP43, Proteintech, 11343-1-AP, 1:750). Sections were washed in 0.01M PBS before being incubated in secondary antibody diluted in blocking buffer (GFP Booster Alexa Fluor 488 [Proteintech, gb2AF488], 1:500; goat anti-chicken IgY (H+L) Alexa Fluor 546 [Invitrogen, A-11040], 1:500; goat anti-rabbit IgY (H+L) Alexa Fluor 633 [Invitrogen, A-21070], 1:750). Sections were washed in 0.01M PBS, stained with Hoechst (1:1000 in 0.01M PBS; Invitrogen, H3570), washed in 0.01M PBS, and mounted on slides with Prolong Diamond Antifade Mountant (Invitrogen, P36970).

Images were acquired using the Nikon CSU-W1/SoRa spinning disk confocal microscope with dual cameral Hamamatsu ORCA-FusionBT. 20x images of the PVN were acquired of one plane in z and were 746µm by 746µm. 60x wide field z-stack images were acquired with a step size of 0.2µm and had a length and width dimension of 249.6µm by 249.6µm. Most, if not all, of one side of the PVN was encompassed by the 60x objective field of view, thus resulting in five-six 60x images taken per mouse.

Representative images in figures x, y z: Images were processed with Fiji. Maximal intensity Z projections of 60x images are from at least 170 slices over 34 µm. Image settings were matched within experiments.

Image Analysis of Brain sections

We used Nikon's NIS-Elements Software to automate the segmentation of primary cilia on PVN images and the quantification of MC4R-GFP fluorescence intensities within the segmented

primary cilia. We designed an artificial intelligence-based segmentation process using the NIS.ai module, extending a previously published approach[122] with some new specific goals: eliminate the need for image pre-processing; remove human decisions from the segmentation process; and classify primary cilia as MC4R positive or MC4R negative automatically. Our method allows for unbiased segmentation and quantification of raw 60x z-stack images that does not rely on setting an arbitrary fluorescence threshold to classify cilia with and without MC4R.

Training of convolutional neural network-based segmentation models for primary cilia segmentation in maximum projection of 60X brain images

The segmentation step aims to automatically identify and delimit primary cilia in each image. To achieve this, we used NIS-elements to train AI models to identify neuronal primary cilia in our images. For this we provided the software with 60X wide-field z-stack images containing four acquisition channels: 405 nm for Hoechst, 488 nm for MC4R-GFP, 561 nm for ADCY3, and 647 nm for CEP43. Images in .nd2 format were directly loaded in NIS-elements version 5.4 (Nikon) and a maximum-intensity projection was obtained from each z-stack. Two separate deep-learning-based segmentation models were trained iteratively using the segment.ai module of NIS-elements on a training set of 20 images each containing 20 to 100 cilia:

- The first model was trained to identify all neuronal primary cilia on the maximum intensity projection using the signal from the 488 nm (MC4R-GFP), 561 nm (ADCY3), and 647 nm (CEP43). To achieve this, the model was trained on a human manual segmentation of all cilia positive for ADCY3 and CEP43 signal; or ADCY3, CEP43 and MC4R-GFP signal.

- The second model was similarly trained to identify only MC4R-GFP positive cilia on the maximum intensity projection using the signal from the 488 nm (MC4R-GFP) and 647 nm (CEP43). To achieve this, the model was trained on human manual segmentation of all cilia positive for MC4R-GFP and CEP43 signal.

To maximize the specificity of the segmentation for downstream analysis, MC4R-positive cilia were defined as objects identified by both segmentation models.

Automated quantification of MC4R localization at the primary cilium in brain

To be able to quantify MC4R localization on large batches of images simultaneously, we designed a NIS GA3 recipe to fully automate the quantification process (Supplemental Fig. 1). First, ADCY3 and CEP43 containing objects with or without MC4R are segmented on a maximum intensity projection of each raw image, using the two segmentation models described above. Segmented objects are stored in two binary layers: MC4R positive object layer and MC4R negative objects layer. To avoid a bias in fluorescence quantification due to the maximum projection and account for total MC4R fluorescence, the two binaries are then copied to a sum intensity projection of the original z-stack image which is used for downstream fluorescence measurements. Objects touching the image borders are removed to avoid quantification of cropped objects. The sum

intensity of pixels in the 488 nm (MC4R-GFP) is then calculated for each object and reported in an output table for each image, along with pixel area.

Because the background fluorescence is often heterogeneous in confocal wide-field images, we also included a measure of the local background fluorescence in the GA3 recipe. More specifically, each object is dilated in 2D to obtain a region directly around the cilium. Fluorescence sum intensity is measured in this background region and reported for each object in the output table along with the area of the background region.

Last, quantification output tables from all images are merged and processed for statistical analysis with R[123]. Objects with a length lower than 3 µm are excluded from the final list of cilia for downstream analysis. The 3µm threshold was set to account for the inclusion of CEP43 signal within the segmented cilia and to improve the specificity of our segmentation protocol. Then fluorescence sum intensity values of each cilium are corrected to account for local background fluorescence: for each cilium, the expected background fluorescence inside the cilium is calculated from the local background area measurement for MC4R-GFP as described in equation 1.

$$\text{(Eq.1) Expected background sum intensity inside cilium} = \frac{\text{Background sum intensity} \times \text{Cilium Area}}{\text{Background Area}}$$

For each cilium, this expected background fluorescence value is then subtracted from the raw fluorescence sum intensities (equation 2). Negative values are set to zero. This corrected sum intensity is referred to as immunofluorescence intensity in the text.

$$\text{(Eq. 2) Corrected sum intensity} = \text{Raw sum intensity} - \text{Expected background sum intensity}$$

Outlier fluorescence values are removed by filtering out cilia with fluorescence above the 99.5th percentile. All fluorescence intensity values were divided by $1e^{+6}$ in graphs for easier visualization of data.

MC4R positive cilia are then grouped by individual mouse and experimental condition, and their corrected sum intensities are plotted as super-plots[124] using ggplot2[125].

Validation of the NIS.ai cilia segmentation algorithm

To evaluate the biological significance of our automated cilia identification method, we tested the agreement between our AI models and manual segmentation of cilia by human researchers from our team. Two PVN images from different mice stained for ADCY3, CEP43, and MC4R-GFP were manually segmented by two researchers for all neuronal cilia and MC4R-GFP positive neuronal cilia. The two researchers reached a consensus on objects identified as neuronal and MC4R-GFP positive cilia in the manual segmentation that the AI was compared to (supplemental figure 2a). These images were independently processed by our AI assisted algorithms to identify neuronal cilia and MC4R-GFP positive neuronal cilia (supplemental figure 2a, b). Researchers were blind to

the AI algorithms results at the time of manual segmentation and the images used had not been used to train the AI segmentation models.

Predictive performances were calculated separately for the AI model identifying all neuronal cilia and the one identifying MC4R-GFP positive cilia, using the corresponding human-segmented binary as the gold standard. To reproduce our main analysis workflow only cilia with a length greater or equal to 3µm were kept for the analysis. A true positive (TP) was defined as an object identified as a cilium both by the AI model and the human operator. A false positive (FP) was defined as an object identified as a cilium by the AI model but not by the human operators. A false negative (FN) was defined as an object defined as a cilium by the human operators but not by the AI-model. The recall and precision of the two AI models compared with the human consensus was calculated from the sizes of these categories according to the following formulas. Recall = TP / (TP + FN) ; Precision = TP/(TP + FP).

For the identification of neuronal cilia, recall was 0.89 and precision was 0.96 (supplemental figure 3c). For the identification of MC4R-GFP positive cilia, recall was 0.97 and precision was 0.79 (supplemental figure 3d).

To further evaluate the robustness of our cilia segmentation protocol, we assessed the specificity of the final segmented primary cilia. To evaluate this, we fasted one *Mc4r*$^{Gfp/Gfp}$ (positive control mouse), and two wildtype mice for 24hrs (negative control mice). We stained two sections of the fasted *Mc4r*$^{Gfp/Gfp}$ mouse (slices were taken from Bregma=-0.82) for ADCY3, CEP43, MC4R-GFP. One section from each wildtype mouse (from Bregma=-0.82) was separated and put through the staining process for ADCY3, CEP43, and MC4R-GFP but the primary antibodies were not added. Both PVNs on each section were imaged (2 images per section). Four positive control and four negative control images (no primary staining) were put through our automatic segmentation protocol. The number of MC4R positive and MC4R negative cilia detected in each image was counted. Because our segmentation protocol identifies cilia in our positive control images but not in negative control images, we concluded that segmented cilia were specific of the primary antibody staining for the MC4R-GFP positive neuronal cilia (supplemental figure 3e).

Assessment of ligand dependent MC4R localization in Cell Culture

A stable, isogenic, clonal IMCD3 cell line expressing MRAP2-3xFLAG and MC4R-3xNeonGreen separated by a T2A self-cleaving peptide under the control of a TATA-less EF1 promoter was established using the FlpIn system (Thermo Fisher Scientific). Cells were grown on acid-washed 12 mm #1.5 cover glass (Fisherbrand, Thermo Fisher Scientific) in DMEM/F12 (11330–057; Gibco) supplemented with 10% FBS (Gemini Bio-products), 100 U/ml penicillin-streptomycin (Gemini Bio-products), and 2 mM L-glutamine (Gemini Bio-products); at a density of 50,000 cells per well of a 24-well plate. Ciliation was induced 24 h after seeding by serum starvation in media containing 0.2% FBS for 24 h. Human AgRP (003-53; Phoenix Pharmaceuticals) diluted in water or

an equivalent volume of water were added at the onset of starvation to a final concentration of 50 nM.

Cells were fixed in phosphate buffered saline (PBS) containing 4% paraformaldehyde (Electron Microscopy Sciences) for 15 minutes at 37ºC. Cells were then permeabilized in PBS containing 0.1% Triton X-100 (BP151-500, Thermo Fisher Scientific), 5% normal donkey serum (017-000-121, Jackson ImmunoResearch), and 3% BSA (BP1605-100, Thermo Fisher Scientific) for 30 minutes. Permeabilized cells were incubated with mouse IgG2b monoclonal anti–acetylated tubulin antibody [T6793, Sigma-Aldrich, 1:1,000 for 1 hour, washed with PBS, and incubated with dye-coupled secondary antibodies (Jackson ImmunoResearch) for 30 minutes. Cells were then washed with PBS, stained with Hoechst 33258, and washed with PBS before mounting with Fluoromount G (Electron Microscopy Sciences). MC4R-3xNeonGreen was detected via the intrinsic fluorescence of NeonGreen.

Cells were imaged in a widefield fluorescence DeltaVision microscope (Applied Precision) equipped with a PlanApo 60×/1.40NA objective lens (Olympus), a pco.edge 4.2 sCMOS camera, a solid state illumination module (Insight), and a Quad polycroic (Chroma). Z stacks with 0.2 µm separation between planes were acquired using SoftWoRx. The illumination settings were: 140 µW 390 nm wavelength for 0.2 seconds to image Hoechst, 222 µW 475 nm wavelength for 0.5 seconds to MC4R-3xNeonGreen, 123 µW 543 nm wavelength for 0.2 seconds to image Cy3-stained acetylated tubulin. Images were flat field corrected, background subtracted, and maximally projected using Fiji. Ciliary intensity and length measurements were taken in maximally projected images using Fiji as previously published[126]. Confocal images shown in figure 4F were acquired with an Airyscan LSM900 (Zeiss).

Quantification of Statistical analysis

Sample sizes were chosen based upon the estimated effect size drawn for previous publications and from the performed experiments. Statistical analyses performed were described in figure legends. Briefly, mean differences of immunofluorescence intensity between conditions are tested by a Welch t-test on the mice's individual means rather than on all cilia, as recommended in the super-plot methodology[3]. Pearson’s correlation coefficient was calculated to test the correlation between MC4R-GFP immunofluorescence and serum leptin levels. Unpaired t-test and/or Welch t-test was conducted on AGRP treatment of cells in vitro. Differences in the proportion of MC4R positive cilia per image in each condition is tested by χ^2 test. Parametric unpaired t-test or one-way ANOVA was conducted on body weight change data. And one way ANOVA was conducted on measured serum leptin levels. A p-value ≤ 0.05 was considered as statistically significant. All data were analyzed using Prism 9.5.0 (GraphPad Software) or R.

Chapter 3: Final Conclusions and Future Directions

We have demonstrated that MC4R localization at the primary cilium is dynamic and reflects energy status and could be the basis for how the brain encodes energy homeostasis. In satiated mice, MC4R levels at the primary cilium is low. However, in mice under energy deficit, MC4R accumulates at the primary cilium. This dynamic change in localization is dependent on leptin and AGRP levels. This provides the molecular basis for encoding information from volumetric signaling and storing information on long term energy homeostasis. Our model only describes how the brain represents information on energy deficit, further studies are needed to elucidate what happens to MC4R localization under high fat diet feeding and obesity; and how body weight set point is determined in development. Future studies should be conducted to investigate whether manipulating MC4R localization at the primary cilium can decrease body weight set point and promote weight loss. Whether other GPCR localization at the primary cilium is involved in information encoding should also be studied.

We have demonstrated that primary cilia on MC4R neurons is necessary for the control of food intake and energy balance by MC4R neurons; MC4R localization at the primary cilium is necessary for the maintenance of long-term energy homeostasis; and that blocking Gs signaling at the primary cilia of PVN^{MC4R} neurons causes hyperphagia and obesity[57,63]. Our data heavily suggests that MC4R signals at the primary cilium to signal satiety. However, during times of satiety, when MC4R is signaling, there are very little MC4R localized at the primary cilium (figure 1), which begs the question of whether MC4R really signals at the primary cilium. There is evidence that changes in ciliary cAMP level are independent from cellular cAMP levels and that changes in ciliary cAMP conveys different messages than changes in cellular cAMP levels[127,128]. More studies are needed to further elucidate whether MC4R signals at the primary cilium *in vivo*; the MC4R signaling cascade after cAMP production; and how ciliary cAMP pools, and not cellular cAMP pools, affect energy homeostasis.

Our data suggests that MC4R trafficking to and from the cilium is important for the regulation of energy balance. Thus, mutations in proteins involved in MC4R trafficking to and from the primary cilium could affect energy balance. By crossing *Mc4r-Gfp* allele with knock out alleles of obesity associated ciliary genes (for example, *Bbs* genes, *Alms1*, or *Inpp5e*) or knocking down obesity associated ciliary genes in *Mc4r-Gfp* mice, we can deduce whether mutations in these genes cause obesity via alterations in MC4R localization.

MC4R neurons respond to both short term and long term anorexigenic and orexigenic signals: MC4R neuron activation and inhibition in response to short term signals from AGRP neurons (and seen in chemogenetic and optogenetic experiments), and long term MC4R protein activation via AGRP and αMSH signaling[48,100,101,107]. How MC4R neurons consolidate these signals is unknown. There is evidence that primary cilia signaling affects neuronal projection formation[129–131]. In the hippocampus, MC4R activation enhances the abundance of AMPA receptors in synapses[132]. The

process of synaptic consolidation involves a cAMP/PKA signaling cascade that eventually leads to transcriptional changes by pCREB[84]. This provides a basis in which MC4R signaling could lead to changes in MC4R neuron projections, and MC4R neuron firing; thus long-term energy homeostasis signals could affect short term energy status signals. However, it remains a question of whether MC4R signaling results in transcriptomic changes that allow for alterations in MC4R projections.

A recently published paper suggests MC4R positive cilia shorten with age and chronic stimulation; and that the shortening of cilia, thus less MC4R at primary cilia, blunts satiety signals thus resulting in obesity and leptin resistance[56]. However, our data shows that increased MC4R levels at primary cilia is leptin and AGRP dependent; and reflects physiological energy stores. Our data suggests that in a hyperphagic state, there is more MC4R localization at the primary cilium; however, Oya et al suggests that in a hyperphagic state, there are shorter cilia, thus less MC4R localized at the primary cilium. Past studies have also focused on primary cilia length and its effects on leptin sensitivity in the hypothalamus[133]. Further experiments should address the question of whether MC4R positive cilia shorten with age or whether there are just less MC4R content in the primary cilium; and whether cilia length, rather than cilia protein composition, is an accurate reflection of the ability of primary cilia to signal.

Figures

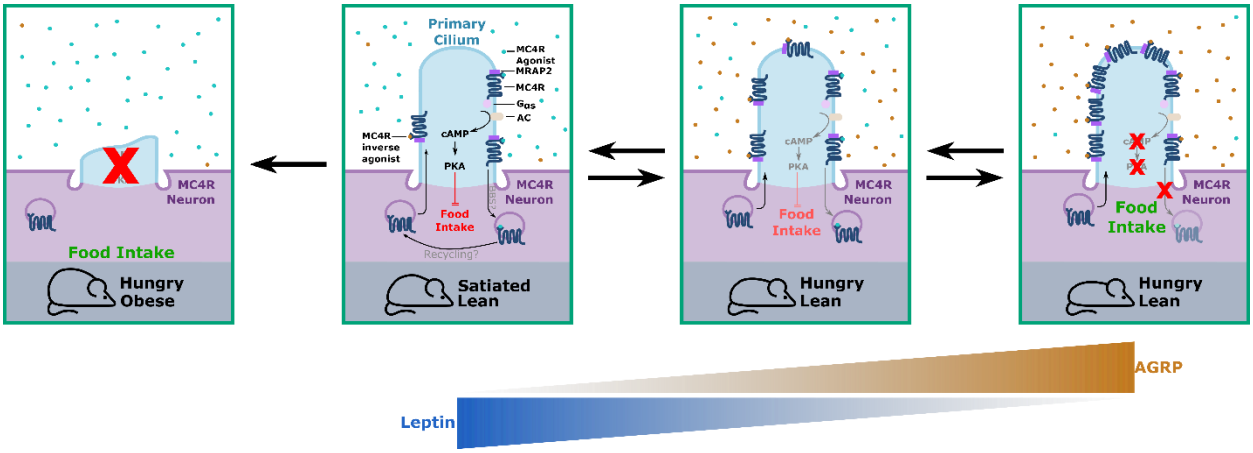


Figure 3.1 Neuronal encoding of energy homeostasis.

References

1. Elmaleh-Sachs, A. *et al.* Obesity Management in Adults: A Review. *JAMA* **330**, 2000–2015 (2023).

2. Suran, M. As Ozempic's Popularity Soars, Here's What to Know About Semaglutide and Weight Loss. *JAMA* **329**, 1627–1629 (2023).

3. Friedman, J. M. A War on Obesity, Not the Obese. *Science* **299**, 856–858 (2003).

4. Silventoinen, K., Rokholm, B., Kaprio, undefined J. & Sørensen, T. I. A. The genetic and environmental influences on childhood obesity: a systematic review of twin and adoption studies. *Int. J. Obes.* **34**, 29–40 (2010).

5. Ahituv, N. *et al.* Medical Sequencing at the Extremes of Human Body Mass. *Am. J. Hum. Genet.* **80**, 779–791 (2007).

6. Benzinou, M. *et al.* Common nonsynonymous variants in PCSK1 confer risk of obesity. *Nat. Genet.* **40**, 943–945 (2008).

7. Loos, R. J. F. *et al.* Common variants near MC4R are associated with fat mass, weight and risk of obesity. *Nat. Genet.* **40**, 768–775 (2008).

8. Willer, C. J. *et al.* Six new loci associated with body mass index highlight a neuronal influence on body weight regulation. *Nat. Genet.* **41**, 25–34 (2009).

9. Loos, R. J. F. & Yeo, G. S. H. The bigger picture of FTO: the first GWAS-identified obesity gene. *Nat. Rev. Endocrinol.* **10**, 51–61 (2014).

10. Aslan, I. R., Ranadive, S. A. & Vaisse, C. Monogenic Disorders Within the Energy Balance Pathway. in *Obesity Before Birth: Maternal and prenatal influences on the offspring* (ed. Lustig, R. H.) 53–69 (Springer US, Boston, MA, 2011). doi:10.1007/978-1-4419-7034-3_3.

11. Speakman, J. R. *et al.* Set points, settling points and some alternative models: theoretical options to understand how genes and environments combine to regulate body adiposity. *Dis. Model. Mech.* **4**, 733–745 (2011).

12. Kennedy, G. C. The role of depot fat in the hypothalamic control of food intake in the rat. *Proc. R. Soc. Lond. B Biol. Sci.* **140**, 578–596 (1953).

13. David S. Weigle *et al.* Effect of fasting, refeeding, and dietary fat restriction on plasma leptin levels - PubMed. *J. Clin. Endocrinol. Metab.* **82**, 561–565 (1997).

14. Yeo, G. S. H. *et al.* The melanocortin pathway and energy homeostasis: From discovery to obesity therapy. *Mol. Metab.* **48**, 101206 (2021).

15. Friedman, J. 20 years of leptin: leptin at 20: an overview. *J. Endocrinol.* **223**, T1-8 (2014).

16. Coleman, D. L. A historical perspective on leptin. *Nat. Med.* **16**, 1097–1099 (2010).

17. Zhang, Y. *et al.* Positional cloning of the mouse obese gene and its human homologue. *Nature* **372**, 425–432 (1994).

18. Tartaglia, L. A. *et al.* Identification and expression cloning of a leptin receptor, OB-R. *Cell* **83**, 1263–1271 (1995).

19. Münzberg, H. & Morrison, C. D. Structure, production and signaling of leptin. *Metabolism* **64**, 13–23 (2015).

20. Cottrell, E. C. & Mercer, J. G. Leptin receptors. *Handb. Exp. Pharmacol.* 3–21 (2012) doi:10.1007/978-3-642-24716-3_1.

21. Stratigopoulos, G. *et al.* Hypomorphism of Fto and Rpgrip1l causes obesity in mice. *J. Clin. Invest.* **126**, 1897–1910.

22. Deem, J. D., Faber, C. L. & Morton, G. J. AgRP neurons: Regulators of feeding, energy expenditure, and behavior. *FEBS J.* **289**, 2362–2381 (2022).

23. Gropp, E. *et al.* Agouti-related peptide–expressing neurons are mandatory for feeding. *Nat. Neurosci.* **8**, 1289–1291 (2005).

24. Luquet, S., Perez, F. A., Hnasko, T. S. & Palmiter, R. D. NPY/AgRP Neurons Are Essential for Feeding in Adult Mice but Can Be Ablated in Neonates. *Science* **310**, 683–685 (2005).

25. Wu, Q., Howell, M. P. & Palmiter, R. D. Ablation of Neurons Expressing Agouti-Related Protein Activates Fos and Gliosis in Postsynaptic Target Regions. *J. Neurosci.* **28**, 9218–9226 (2008).

26. Qian, S. *et al.* Neither Agouti-Related Protein nor Neuropeptide Y Is Critically Required for the Regulation of Energy Homeostasis in Mice. *Mol. Cell. Biol.* **22**, 5027–5035 (2002).

27. Atasoy, D., Betley, J. N., Su, H. H. & Sternson, S. M. Deconstruction of a neural circuit for hunger. *Nature* **488**, 172–177 (2012).

28. Krashes, M. J. *et al.* Rapid, reversible activation of AgRP neurons drives feeding behavior in mice. *J. Clin. Invest.* **121**, 1424–1428 (2011).

29. Aponte, Y., Atasoy, D. & Sternson, S. M. AGRP neurons are sufficient to orchestrate feeding behavior rapidly and without training. *Nat. Neurosci.* **14**, 351–355 (2011).

30. Han, Y. *et al.* Deciphering an AgRP-serotoninergic neural circuit in distinct control of energy metabolism from feeding. *Nat. Commun.* **12**, 3525 (2021).

31. Ahn, B. H., Kim, M. & Kim, S.-Y. Brain circuits for promoting homeostatic and non-homeostatic appetites. *Exp. Mol. Med.* **54**, 349–357 (2022).

32. Atasoy, D. *et al.* A genetically specified connectomics approach applied to long-range feeding regulatory circuits. *Nat. Neurosci.* **17**, 1830–1839 (2014).

33. Biglari, N. *et al.* Functionally distinct POMC-expressing neuron subpopulations in hypothalamus revealed by intersectional targeting. *Nat. Neurosci.* **24**, 913–929 (2021).

34. Zhan, C. POMC Neurons: Feeding, Energy Metabolism, and Beyond. in *Neural Regulation of Metabolism* (eds. Wu, Q. & Zheng, R.) 17–29 (Springer, Singapore, 2018). doi:10.1007/978-981-13-1286-1_2.

35. Krude, H. *et al.* Severe early-onset obesity, adrenal insufficiency and red hair pigmentation caused by POMC mutations in humans. *Nat. Genet.* **19**, 155–157 (1998).

36. Yaswen, L., Diehl, N., Brennan, M. B. & Hochgeschwender, U. Obesity in the mouse model of pro-opiomelanocortin deficiency responds to peripheral melanocortin. *Nat. Med.* **5**, 1066–1070 (1999).

37. Balthasar, N. *et al.* Leptin receptor signaling in POMC neurons is required for normal body weight homeostasis. *Neuron* **42**, 983–991 (2004).

38. Lam, D. D. *et al.* Conditional expression of Pomc in the Lepr-positive subpopulation of POMC neurons is sufficient for normal energy homeostasis and metabolism. *Endocrinology* **156**, 1292–1302 (2015).

39. Li, H. *et al.* The melanocortin action is biased toward protection from weight loss in mice. *Nat. Commun.* **14**, 2200 (2023).

40. Lubrano-Berthelier, C., Le Stunff, C., Bougnères, P. & Vaisse, C. A homozygous null mutation delineates the role of the melanocortin-4 receptor in humans. *J. Clin. Endocrinol. Metab.* **89**, 2028–2032 (2004).

41. Vaisse, C., Clement, K., Guy-Grand, B. & Froguel, P. A frameshift mutation in human MC4R is associated with a dominant form of obesity. *Nat. Genet.* **20**, 113–114 (1998).

42. Lubrano-Berthelier, C. *et al.* Molecular genetics of human obesity-associated MC4R mutations. *Ann. N. Y. Acad. Sci.* **994**, 49–57 (2003).

43. Calton, M. A. *et al.* Association of functionally significant Melanocortin-4 but not Melanocortin-3 receptor mutations with severe adult obesity in a large North American case-control study. *Hum. Mol. Genet.* **18**, 1140–1147 (2009).

44. Vaisse, C. *et al.* Melanocortin-4 receptor mutations are a frequent and heterogeneous cause of morbid obesity. *J. Clin. Invest.* **106**, 253–262 (2000).

45. Balthasar, N. *et al.* Divergence of melanocortin pathways in the control of food intake and energy expenditure. *Cell* **123**, 493–505 (2005).

46. Matharu, N. *et al.* CRISPR-mediated activation of a promoter or enhancer rescues obesity caused by haploinsufficiency. *Science* **363**, (2019).

47. Shah, B. P. *et al.* MC4R-expressing glutamatergic neurons in the paraventricular hypothalamus regulate feeding and are synaptically connected to the parabrachial nucleus. *Proc. Natl. Acad. Sci. U. S. A.* **111**, 13193–13198 (2014).

48. Garfield, A. S. *et al.* A neural basis for melanocortin-4 receptor regulated appetite. *Nat. Neurosci.* **18**, 863–871 (2015).

49. Ferraz Barbosa, B. *et al.* Efficacy and Safety of Setmelanotide, a Melanocortin-4 Receptor Agonist, for Obese Patients: A Systematic Review and Meta-Analysis. *J. Pers. Med.* **13**, 1460 (2023).

50. Chen, K. Y. *et al.* RM-493, a Melanocortin-4 Receptor (MC4R) Agonist, Increases Resting Energy Expenditure in Obese Individuals. *J. Clin. Endocrinol. Metab.* **100**, 1639–1645 (2015).

51. Kievit, P. *et al.* Chronic Treatment With a Melanocortin-4 Receptor Agonist Causes Weight Loss, Reduces Insulin Resistance, and Improves Cardiovascular Function in Diet-Induced Obese Rhesus Macaques. *Diabetes* **62**, 490–497 (2013).

52. Krashes, M. J., Lowell, B. B. & Garfield, A. S. Melanocortin-4 receptor-regulated energy homeostasis. *Nat. Neurosci.* **19**, 206–219 (2016).

53. Seo, S. *et al.* BBS6, BBS10, and BBS12 form a complex with CCT/TRiC family chaperonins and mediate BBSome assembly. *Proc. Natl. Acad. Sci.* **107**, 1488–1493 (2010).

54. Siljee, J. E. *et al.* Subcellular localization of MC4R with ADCY3 at neuronal primary cilia underlies a common pathway for genetic predisposition to obesity. *Nat. Genet.* **50**, 180–185 (2018).

55. Saeed, S. *et al.* Loss-of-function mutations in ADCY3 cause monogenic severe obesity. *Nat. Genet.* **50**, 175–179 (2018).

56. Oya, M. *et al.* Age-related ciliopathy: Obesogenic shortening of melanocortin-4 receptor-bearing neuronal primary cilia. *Cell Metab.* **36**, 1044-1058.e10 (2024).

57. Wang, Y. *et al.* Melanocortin 4 receptor signals at the neuronal primary cilium to control food intake and body weight. *J. Clin. Invest.* **131**, (2021).

58. Sebag, J. A., Zhang, C., Hinkle, P. M., Bradshaw, A. M. & Cone, R. D. Developmental control of the melanocortin-4 receptor by MRAP2 proteins in zebrafish. *Science* **341**, 278–281 (2013).

59. Asai, M. *et al.* Loss of Function of the Melanocortin 2 Receptor Accessory Protein 2 Is Associated with Mammalian Obesity. *Science* **341**, 275–278 (2013).

60. Schonnop, L. *et al.* Decreased melanocortin-4 receptor function conferred by an infrequent variant at the human melanocortin receptor accessory protein 2 gene. *Obes. Silver Spring Md* **24**, 1976–1982 (2016).

61. Geets, E. *et al.* Copy number variation (CNV) analysis and mutation analysis of the 6q14.1-6q16.3 genes SIM1 and MRAP2 in Prader Willi like patients. *Mol. Genet. Metab.* **117**, 383–388 (2016).

62. Baron, M. *et al.* Loss-of-function mutations in MRAP2 are pathogenic in hyperphagic obesity with hyperglycemia and hypertension. *Nat. Med.* **25**, 1733–1738 (2019).

63. Bernard, A. *et al.* MRAP2 regulates energy homeostasis by promoting primary cilia localization of MC4R. *JCI Insight* **8**, (2023).

64. Wu, Y., Zhou, J. & Yang, Y. Peripheral and central control of obesity by primary cilia. *J. Genet. Genomics* **50**, 295–304 (2023).

65. Reiter, J. F. & Leroux, M. R. Genes and molecular pathways underpinning ciliopathies. *Nat. Rev. Mol. Cell Biol.* **18**, 533–547 (2017).

66. Yang, D. J., Hong, J. & Kim, K. W. Hypothalamic primary cilium: A hub for metabolic homeostasis. *Exp. Mol. Med.* **53**, 1109–1115 (2021).

67. Long, H. & Huang, K. Transport of Ciliary Membrane Proteins. *Front. Cell Dev. Biol.* **7**, (2020).

68. Tomlinson, J. W. Bardet-Biedl syndrome: A focus on genetics, mechanisms and metabolic dysfunction. *Diabetes Obes. Metab.* **26**, 13–24 (2024).

69. Brewer, K. M., Brewer, K. K., Richardson, N. C. & Berbari, N. F. Neuronal cilia in energy homeostasis. *Front. Cell Dev. Biol.* **10**, (2022).

70. Gupta, N., D'Acierno, M., Zona, E., Capasso, G. & Zacchia, M. Bardet-Biedl syndrome: The pleiotropic role of the chaperonin-like BBS6, 10, and 12 proteins. *Am. J. Med. Genet. C Semin. Med. Genet.* **190**, 9–19 (2022).

71. Oh, E. C., Vasanth, S. & Katsanis, N. Metabolic regulation and energy homeostasis through the primary Cilium. *Cell Metab.* **21**, 21–31 (2015).

72. Mihai, C. M., Catrinoiu, D., Marshall, J., Stoicescu, R. & Tofolean, I. T. Cilia, Alström syndrome--molecular mechanisms and therapeutic perspectives. *J. Med. Life* **1**, 254–261 (2008).

73. Girard, D. & Petrovsky, N. Alström syndrome: insights into the pathogenesis of metabolic disorders. *Nat. Rev. Endocrinol.* **7**, 77–88 (2011).

74. Geberhiwot, T. *et al.* Relative Adipose Tissue Failure in Alström Syndrome Drives Obesity-Induced Insulin Resistance. *Diabetes* **70**, 364–376 (2020).

75. Larkins, C. E., Aviles, G. D. G., East, M. P., Kahn, R. A. & Caspary, T. Arl13b regulates ciliogenesis and the dynamic localization of Shh signaling proteins. *Mol. Biol. Cell* **22**, 4694–4703 (2011).

76. Qiu, H., Fujisawa, S., Nozaki, S., Katoh, Y. & Nakayama, K. Interaction of INPP5E with ARL13B is essential for its ciliary membrane retention but dispensable for its ciliary entry. *Biol. Open* **10**, bio057653 (2021).

77. Terry, T. T. *et al.* Ciliary ARL13B prevents obesity in mice. 2023.08.02.551695 Preprint at https://doi.org/10.1101/2023.08.02.551695 (2023).

78. Lee, H., Song, J., Jung, J. H. & Ko, H. W. Primary cilia in energy balance signaling and metabolic disorder. *BMB Rep.* **48**, 647–654 (2015).

79. Mukhopadhyay, S. *et al.* TULP3 bridges the IFT-A complex and membrane phosphoinositides to promote trafficking of G protein-coupled receptors into primary cilia. *Genes Dev.* **24**, 2180–2193 (2010).

80. Sun, X. *et al.* Tubby is required for trafficking G protein-coupled receptors to neuronal cilia. *Cilia* **1**, 21 (2012).

81. Gianni, G. & Pasqualetti, M. Wiring and Volume Transmission: An Overview of the Dual Modality for Serotonin Neurotransmission. *ACS Chem. Neurosci.* **14**, 4093–4104 (2023).

82. Agnati, L. F. *et al.* A correlation analysis of the regional distribution of central enkephalin and beta-endorphin immunoreactive terminals and of opiate receptors in adult and old male rats. Evidence

for the existence of two main types of communication in the central nervous system: the volume transmission and the wiring transmission. *Acta Physiol. Scand.* **128**, 201–207 (1986).

83. Liu, C., Goel, P. & Kaeser, P. S. Spatial and temporal scales of dopamine transmission. *Nat. Rev. Neurosci.* **22**, 345–358 (2021).

84. Asok, A., Leroy, F., Rayman, J. B. & Kandel, E. R. Molecular Mechanisms of the Memory Trace. *Trends Neurosci.* **42**, 14–22 (2019).

85. Titley, H. K., Brunel, N. & Hansel, C. Toward a Neurocentric View of Learning. *Neuron* **95**, 19–32 (2017).

86. Ersoy, B. A. *et al.* Mechanism of N-terminal modulation of activity at the melanocortin-4 receptor GPCR. *Nat. Chem. Biol.* **8**, 725–730 (2012).

87. Abdel-Malek, Z. A. Melanocortin receptors: their functions and regulation by physiological agonists and antagonists. *Cell. Mol. Life Sci. CMLS* **58**, 434–441 (2001).

88. Ellacott, K. L. J. & Cone, R. D. The role of the central melanocortin system in the regulation of food intake and energy homeostasis: lessons from mouse models. *Philos. Trans. R. Soc. Lond. B. Biol. Sci.* **361**, 1265–1274 (2006).

89. Garfield, A. S., Lam, D. D., Marston, O. J., Przydzial, M. J. & Heisler, L. K. Role of central melanocortin pathways in energy homeostasis. *Trends Endocrinol. Metab. TEM* **20**, 203–215 (2009).

90. Morton, G. J., Cummings, D. E., Baskin, D. G., Barsh, G. S. & Schwartz, M. W. Central nervous system control of food intake and body weight. *Nature* **443**, 289–295 (2006).

91. Cowley, M. A. *et al.* Integration of NPY, AGRP, and melanocortin signals in the hypothalamic paraventricular nucleus: evidence of a cellular basis for the adipostat. *Neuron* **24**, 155–163 (1999).

92. Cowley, M. A. *et al.* Leptin activates anorexigenic POMC neurons through a neural network in the arcuate nucleus. *Nature* **411**, 480–484 (2001).

93. Balthasar, N. *et al.* Leptin receptor signaling in POMC neurons is required for normal body weight homeostasis. *Neuron* **42**, 983–991 (2004).

94. Cone, R. D. Anatomy and regulation of the central melanocortin system. *Nat. Neurosci.* **8**, 571–578 (2005).

95. Millington, G. W. The role of proopiomelanocortin (POMC) neurones in feeding behaviour. *Nutr. Metab.* **4**, 18 (2007).

96. Mandelblat-Cerf, Y. *et al.* Arcuate hypothalamic AgRP and putative POMC neurons show opposite changes in spiking across multiple timescales. *eLife* **4**, e07122 (2015).

97. Krashes, M. J., Shah, B. P., Koda, S. & Lowell, B. B. Rapid versus delayed stimulation of feeding by the endogenously released AgRP neuron mediators GABA, NPY, and AgRP. *Cell Metab.* **18**, 588–595 (2013).

98. Chen, Y., Lin, Y.-C., Kuo, T.-W. & Knight, Z. A. Sensory detection of food rapidly modulates arcuate feeding circuits. *Cell* **160**, 829–841 (2015).

99. Goldstein, N. *et al.* Hypothalamic detection of macronutrients via multiple gut-brain pathways. *Cell Metab.* **33**, 676-687.e5 (2021).

100. Beutler, L. R. *et al.* Dynamics of Gut-Brain Communication Underlying Hunger. *Neuron* **96**, 461-475.e5 (2017).

101. Aponte, Y., Atasoy, D. & Sternson, S. M. AGRP neurons are sufficient to orchestrate feeding behavior rapidly and without training. *Nat. Neurosci.* **14**, 351–355 (2011).

102. Deem, J. D., Faber, C. L. & Morton, G. J. AgRP neurons: Regulators of feeding, energy expenditure, and behavior. *FEBS J.* **289**, 2362–2381 (2022).

103. Krashes, M. J. *et al.* Rapid, reversible activation of AgRP neurons drives feeding behavior in mice. *J. Clin. Invest.* **121**, 1424–1428 (2011).

104. Coleman, D. L. A historical perspective on leptin. *Nat. Med.* **16**, 1097–1099 (2010).

105. Friedman, J. 20 YEARS OF LEPTIN: Leptin at 20: an overview. *J. Endocrinol.* **223**, T1–T8 (2014).

106. Hahn, T. M., Breininger, J. F., Baskin, D. G. & Schwartz, M. W. Coexpression of Agrp and NPY in fasting-activated hypothalamic neurons. *Nat. Neurosci.* **1**, 271–272 (1998).

107. Chen, Y. *et al.* Sustained NPY signaling enables AgRP neurons to drive feeding. *eLife* https://elifesciences.org/articles/46348/figures (2019) doi:10.7554/eLife.46348.

108. Guemez-Gamboa, A., Coufal, N. G. & Gleeson, J. G. Primary cilia in the developing and mature brain. *Neuron* **82**, 511–521 (2014).

109. Mykytyn, K. & Askwith, C. G-Protein-Coupled Receptor Signaling in Cilia. *Cold Spring Harb. Perspect. Biol.* **9**, (2017).

110. Veland, I. R., Awan, A., Pedersen, L. B., Yoder, B. K. & Christensen, S. T. Primary cilia and signaling pathways in mammalian development, health and disease. *Nephron Physiol.* **111**, p39-53 (2009).

111. Pan, J., Wang, Q. & Snell, W. J. Cilium-generated signaling and cilia-related disorders. *Lab. Investig. J. Tech. Methods Pathol.* **85**, 452–463 (2005).

112. Schou, K. B., Pedersen, L. B. & Christensen, S. T. Ins and outs of GPCR signaling in primary cilia. *EMBO Rep.* **16**, 1099–1113 (2015).

113. Bangs, F. & Anderson, K. V. Primary Cilia and Mammalian Hedgehog Signaling. *Cold Spring Harb. Perspect. Biol.* **9**, (2017).

114. Taber, K. H. & Hurley, R. A. Volume Transmission in the Brain: Beyond the Synapse. *J. Neuropsychiatry Clin. Neurosci.* **26**, iv–4 (2014).

115. Ye, F., Nager, A. R. & Nachury, M. V. BBSome trains remove activated GPCRs from cilia by enabling passage through the transition zone. *J. Cell Biol.* **217**, 1847–1868 (2018).

116. Nachury, M. V. & Mick, D. U. Establishing and regulating the composition of cilia for signal transduction. *Nat. Rev. Mol. Cell Biol.* **20**, 389–405 (2019).

117. Friedman, J. M. Leptin and the endocrine control of energy balance. *Nat. Metab.* **1**, 754–764 (2019).

118. Wu, Q., Howell, M. P., Cowley, M. A. & Palmiter, R. D. Starvation after AgRP neuron ablation is independent of melanocortin signaling. *Proc. Natl. Acad. Sci.* **105**, 2687–2692 (2008).

119. Wu, Q., Howell, M. P. & Palmiter, R. D. Loss of GABAergic signaling by AgRP neurons to the parabrachial nucleus leads to starvation. *Cell* **137**, 1225–1234 (2009).

120. Gianni, G. & Pasqualetti, M. Wiring and Volume Transmission: An Overview of the Dual Modality for Serotonin Neurotransmission. *ACS Chem. Neurosci.* **14**, 4093–4104 (2023).

121. Liu, C., Goel, P. & Kaeser, P. S. Spatial and temporal scales of dopamine transmission. *Nat. Rev. Neurosci.* **22**, 345–358 (2021).

122. Bansal, R. *et al.* Artificial Intelligence Approaches to Assessing Primary Cilia. *J. Vis. Exp. JoVE* 10.3791/62521 (2021) doi:10.3791/62521.

123. R Core Team (2023). R: A language and environment for statistical computing.

124. Lord, S. J., Velle, K. B., Mullins, R. D. & Fritz-Laylin, L. K. SuperPlots: Communicating reproducibility and variability in cell biology. *J. Cell Biol.* **219**, e202001064 (2020).

125. Wickham, H. ggplot2: Elegant Graphics for Data Analysis. (2016).

126. Nager, A. R. *et al.* An Actin Network Dispatches Ciliary GPCRs into Extracellular Vesicles to Modulate Signaling. *Cell* **168**, 252-263.e14 (2017).

127. Jiang, J. Y., Falcone, J. L., Curci, S. & Hofer, A. M. Direct visualization of cAMP signaling in primary cilia reveals up-regulation of ciliary GPCR activity following Hedgehog activation. *Proc. Natl. Acad. Sci.* **116**, 12066–12071 (2019).

128. Sherpa, R. T. *et al.* Sensory primary cilium is a responsive cAMP microdomain in renal epithelia. *Sci. Rep.* **9**, 6523 (2019).

129. Lee, C. H. *et al.* Primary cilia mediate early life programming of adiposity through lysosomal regulation in the developing mouse hypothalamus. *Nat. Commun.* **11**, 5772 (2020).

130. Kumamoto, N. *et al.* A role for primary cilia in glutamatergic synaptic integration of adult-born neurons. *Nat. Neurosci.* **15**, 399–405 (2012).

131. Guo, J. *et al.* Primary Cilia Signaling Shapes the Development of Interneuronal Connectivity. *Dev. Cell* **42**, 286-300.e4 (2017).

132. Shen, Y., Fu, W.-Y., Cheng, E. Y. L., Fu, A. K. Y. & Ip, N. Y. Melanocortin-4 receptor regulates hippocampal synaptic plasticity through a protein kinase A-dependent mechanism. *J. Neurosci. Off. J. Soc. Neurosci.* **33**, 464–472 (2013).

133. Han, Y. M. *et al.* Leptin-promoted cilia assembly is critical for normal energy balance. *J. Clin. Invest.* **124**, 2193–2197 (2014).